

Assessment of Blood-Brain Barrier (BBB) Permeability

CONSIDERATIONS FOR OPTIMIZATION OF THE
PHARMACOKINETIC ANALYSIS OF BLOOD-BRAIN
BARRIER PERMEABILITY

By Ashley GILBANK,

*A Thesis Submitted to the School of Graduate Studies in the Partial
Fulfillment of the Requirements for the Degree Master's of Applied
Science*

McMaster University © Copyright by Ashley GILBANK June 1,
2021

McMaster University

Master's of Applied Science (2021)

Hamilton, Ontario (School of Biomedical Engineering)

TITLE: Considerations for Optimization of the Pharmacokinetic Analysis of Blood-Brain Barrier Permeability

AUTHOR: Ashley GILBANK (McMaster University)

SUPERVISOR: Dr. Michael NOSEWORTHY

NUMBER OF PAGES: ix, 82

Abstract

Dynamic contrast enhanced MR imaging (DCE-MRI) has commonly been used to investigate disruptions in microvascular capillary permeability in pathologies such as tumours, and in brain diseases such as multiple sclerosis. This imaging technique involves intravenous injection of a contrast agent, which can modulate MR signal contrast, while frequently acquiring images (i.e. every few seconds) as the agent perfuses through the tissue of interest. Microvascular permeability, and other parameters such as blood volume and flow (perfusion) can be quantified through application of a pharmacokinetic model on the data acquired from the MRI scan. The model requires input from both the biological (e.g. pharmacokinetic rate constants) as well as physical (i.e. scanner settings) parameters. As there are a great many variables and different biophysical models (e.g. high blood flow, high permeability tissues, etc.) there needs to be considerations made for situations where the permeability may be only slightly different from normal. In the brain the blood-brain barrier (BBB) is a highly selective barrier that restricts most bulk diffusion/permeability of solutes. Changes in BBB permeability is likely only subtle in diseases such as depression or bipolar disorder, especially when compared against hypervascular-hypermemeable cancers that are void of a BBB altogether. The problem is however, to decide which model of BBB permeability is best suited for differentiating subtle changes. Thus the intention of this project was to investigate multiple pharmacokinetic models for the tracking of MRI contrast agent in regions of the brain with an intact BBB. In the brain, where there is strict regulation of molecules passing through the microvasculature into the extracellular space, and where more subtle disruptions might be of interest, different assumptions may be necessary. Four models were investigated: the Tofts model, the modified Tofts model, the two-compartment exchange model, and the uptake model. Scans of eight healthy subjects were analyzed, and permeability was quantified using each model. The accuracy of each model, quantified by the R^2 value, were compared. Analysis found that the Tofts model performed significantly worse than the modified Tofts and Uptake models when fitting regions of the brain with a blood-brain barrier, with a p-value of 0.006. The analysis did not reveal any significant difference between the modified Tofts, Uptake or 2CX models, although perhaps it was obscured due to the limited number of data points. Further investigation is needed to determine any differences between the three top-performing models.

Acknowledgements

I'd like to thank Dr. Michael Noseworthy for the opportunity to work on this project and for guidance throughout. I'd also like to thank the Physician Services Incorporated (PSI) Foundation for their generous funding of this project (Frey et al. 2017). Thanks as well to Norm Konyer for providing assistance many times over the course of this project, as well as writing multiple pre-processing scripts. Another thanks to Kim Desmond who also contributed with the T1-mapping method used in this project. Additionally, thank you to Dr. Frey for heading the clinical study and to Yola El Dahr for her collaboration. Finally, thank you to the members of the Noseworthy lab for providing support and advice along the way.

Contents

Abstract	iii
Acknowledgements	iv
1 Introduction	1
1.1 Introduction	1
1.2 The Blood-Brain Barrier	1
1.3 Assessing Permeability Non-Invasively	2
1.4 Dynamic MRI Scanning Approaches	3
2 Background	5
2.1 MRI Physics	5
2.1.1 Basics	5
2.1.2 Dynamic Contrast Enhanced MRI	7
2.2 Pharmacokinetic Modelling of Microvascular Permeability	8
2.2.1 Two-Compartment Exchange Model	9
2.2.2 Uptake Model	10
2.2.3 The Tofts Model	10
2.2.4 The Modified Tofts Model	11
3 Methods	12
3.1 Subjects	12
3.2 Scan Parameters	12
3.3 Pre-processing	13
3.4 Processing	13
3.4.1 Signal to Concentration	13
3.4.2 Anatomical Regions of Interest	14
3.4.3 Arterial Input Function	14
3.4.4 Model Fitting	16
3.5 Statistical Comparison of Models	17
3.6 Considerations	18
3.6.1 Signal vs. Concentration	19
3.6.2 Registration Interpolation Methods	20

3.6.3	Order of Concentration Calculation	21
4	Results	25
4.1	Tabular Results	25
4.2	Results Figures	26
4.3	Statistical Analysis	31
5	Discussion and Conclusions	36
5.1	Discussion of Results	36
5.2	Significance	38
5.3	Future Directions	39
A	Code	41
A1	Pre-Processing	41
A1.1	Registration with FSL	41
A1.2	Generating T1 Map	47
A2	Processing	51
A2.1	Main Function	51
A2.2	Sub-Functions	53
A2.3	The Four Models	58
A2.4	Processing Multiple Exams	65
A2.5	Consolidating Results	65
B	Data	69
A1	Units and Exam Index	69
A2	Raw Data	70
	Bibliography	80

List of Figures

2.1	Two-Compartment Exchange Model Schematic	9
2.2	Tofts Model Schematic	11
3.1	Bilateral regions of interest	15
3.2	Midline regions of interest	16
3.3	Hippocampus region of interest	17
3.4	Amygdala regions of interest	18
3.5	Example arterial input function	19
3.6	Signal vs. Tracer Concentration	20
3.7	Concentration curves 1	22
3.8	Concentration curves 2	23
3.9	Concentration curves 3	23
3.10	Concentration curves 4	24
4.1	Posterior Pituitary 8173	28
4.2	Right Amygdala 8126	29
4.3	Right Amygdala 8239	29
4.4	Right Amygdala 8264	30
4.5	Left Putamen 8242	30
4.6	ANCOVA Values, Posterior Pituitary	32
4.7	ANCOVA Graph, Posterior Pituitary	33
4.8	Comparison of R^2 Means	34
4.9	ANOVA Values, all BBB ROIs	34
4.10	ANCOVA Values, all BBB ROIs	35
4.11	ANCOVA Graph, all BBB ROIs	35

List of Tables

4.1	Mean R^2	26
4.2	Parameter Unit Index	26
4.3	Mean Permeability Measures	27
4.4	Mean Volume Space Fractions	27
4.5	Mean Plasma Perfusion and MTT	28
4.6	P-values for Model Analysis in ROIs	31
A2.1	Parameter Unit Index	69
A2.2	Subject-Scan Index	70
A2.3	Posterior Pituitary 1	71
A2.4	Posterior Pituitary 2	71
A2.5	Pons 1	71
A2.6	Pons 2	72
A2.7	Cerebellum 1	72
A2.8	Cerebellum 2	72
A2.9	Left Putamen 1	73
A2.10	Left Putamen 2	73
A2.11	Right Putamen 1	73
A2.12	Right Putamen 2	74
A2.13	Left Amygdala 1	74
A2.14	Left Amygdala 2	74
A2.15	Right Amygdala 1	75
A2.16	Right Amygdala 2	75
A2.17	Left Thalamus 1	75
A2.18	Left Thalamus 2	76
A2.19	Right Thalamus 1	76
A2.20	Right Thalamus 2	76
A2.21	Left Head of Caudate Nucleus 1	77
A2.22	Left Head of Caudate Nucleus 2	77
A2.23	Right Head of Caudate Nucleus 1	77
A2.24	Right Head of Caudate Nucleus 2	78
A2.25	Left Hippocampus 1	78
A2.26	Left Hippocampus 2	78
A2.27	Right Hippocampus 1	79

A2.28 Right Hippocampus 2 79

Chapter 1

Introduction

1.1 Introduction

The delivery of oxygen and nutrients to organs is essential to their proper function. This job is maintained by the circulatory system, with blood being the medium for these molecules, and vasculature being the transportation system. Microvasculature also bears the responsibility of restricting harmful toxins or other substances which would be detrimental to these organs. Different organs and tissues have different needs and sensitivities, so their respective vasculature has different properties to regulate what is allowed to permeate through the vessel walls into the surrounding tissue and what isn't. However, normal vessel permeability can be disrupted in some pathologies. Detecting such abnormalities is an area of interest for understanding the mechanisms of these pathologies. In the body most assessment of vascular permeability focuses on tumours where it is well understood that cancers result in hypervascular and hyperpermeable capillaries.

In the brain, the boundary between vasculature and the surrounding tissue is highly regulated by a collection of structural and functional mechanisms, which together are referred to as the **blood-brain barrier (BBB)**. The BBB is a functional barrier at the level of the vascular capillary network. This barrier is vital to normal brain function, and its disruption is characteristic of numerous neurological pathologies, such as multiple sclerosis (MS), Alzheimer's disease (AD), and traumatic brain injuries (TBI). Observing and quantifying the permeability of microvasculature in the brain lends itself to the better understanding of such pathologies, and can aid in diagnosis.

1.2 The Blood-Brain Barrier

The circulatory system is comprised of vasculature which deliver nutrients and oxygen to organs, tissues, and cells throughout the body. These blood vessels branch

off and decrease in size until they reach their destination, where they become small microvasculature through which their contents are exchanged with the surrounding extravascular space, for waste products. Depending on the region in the body, microvasculature has different properties that affects what cells, molecules and ions are allowed to cross their threshold. The strictest of these regulations occur in the brain, from a set of mechanisms labelled “the blood-brain barrier,” or BBB (Daneman and Prat 2015).

The BBB is necessary to restrict toxins and pathogens from entering the brain, maintaining a healthy environment for normal brain function. There are some pathologies, however, which disrupt this barrier and lead to increase leakage into the brain. Such disruption has been observed in multiple sclerosis (MS), stroke, Alzheimer’s disease, epilepsy, and traumatic brain injuries. Recently, bipolar disorder has been hypothesized to have a relation to a degraded BBB (Patel and Frey 2015). This hypothesis has been supported by a recent imaging study (Kamintsky et al. 2020), which detected increased BBB leakage in subjects with bipolar disorder.

1.3 Assessing Permeability Non-Invasively

Imaging technologies can be used to visualize, and even quantify, the permeability of tissue capillaries. Often this is done with the use of contrast agents, but it can also be achieved without. For example, quite recently work using a double echo arterial spin labelling (ASL) sequence, showed that MRI can be used to measure BBB permeability without the introduction of an exogenous agent (Ohene et al. 2021). Nonetheless, apart from this recent work all imaging measures of microvasculature has been done with endogenous contrast agents. Assessment of BBB permeability allows the investigation, and potential grading, of pathologies which disrupt normal capillary function.

Various mathematical models have been developed for quantifying the permeability of capillaries. The models are usually adapted based on tissue type/location (e.g. brain and elsewhere), each with a different set of assumptions about the tissue and vasculature of interest. A previous study has investigated the suitability of four such models—the two-compartment exchange model, the uptake model, the Tofts model and the modified Tofts model—which were applied and compared in cervical tumours, which tend to be highly vascular and permeable.

Due to the strict nature of the BBB and subsequent low permeability, the same assumptions made in a model suitable for tumours does not apply in the brain. In addition, although large disruptions in BBB permeability are easily noted in pathologies such as MS, more subtle disruptions may present in diseases such as

bipolar disorder. The BBB disruption is easily noted in many brain tumours and MS as a profound change in MR image contrast after intravenous injection of a contrast agent such as a gadolinium chelate. In these examples a simple comparison of images taken before and after injection shows obvious difference that isn't routinely modeled (mathematically) when performing diagnostic evaluation. However, with more subtle BBB disruptions pre- and post-injection contrast images are not easily differentiable. Therefore a more detailed assessment is required. This is done through the application of a dynamic scan, that is the assessment of the contrast agent induced signal changes, over time. Dynamic scanning involves rapidly imaging the whole brain every few seconds while a contrast agent perfuses through the tissue. This is then modeled mathematically giving the most accurate method to detect smaller differences in permeability.

1.4 Dynamic MRI Scanning Approaches

As mentioned, other MR imaging techniques are available to investigate the perfusion of substances across the blood-brain barrier (and other vasculature). These include Dynamic Contrast Enhanced (DCE), Dynamic Susceptibility Contrast (DSC), and the aforementioned Arterial Spin Labelling MRI. These techniques differ in their scan length, the physical properties they measure, and how they acquire the perfusion information (McGehee et al. 2012; Essig et al. 2013; Jahng et al. 2014; Elster 2021).

DCE, the technique used in this project, and DSC both use an injection of a gadolinium-based contrast agent. This type of contrast agent has two effects on the hydrogen atoms from which MR acquires its signal. The effect that DCE is based on is T1 relaxation shortening. When the Gd contrast agent is near hydrogen atoms, their T1 relaxation time is shortened, which can be seen as an increase of signal on a T1-weighted scan. The shortening is dependant on local tracer concentration, and therefore the concentration of tracer can be found. The change of concentration over time can be modelled to find how much is crossing through the vasculature, and permeability can be found. These scans typically require 5-10 minutes.

The second effect of gadolinium is that as it passes through vasculature, it creates a distortion in the magnetic field. This results in T2 or T2* dephasing and a subsequent loss of signal, which can also be modelled to find different parameters, such as blood flow, blood volume, and mean transit time (MTT, the average time tracer spends in a compartment). This technique only requires around 2 minutes of scan time.

ASL differs from the previous two methods in that it does not require an injection of a contrast agent, instead tracking endogenous blood-water- that is, the water that is naturally present in blood. It achieves this by "magnetically labelling" water molecules in blood vessels, and then tracks the signal as the water passes out of the vasculature. The signal decreases proportionally to the perfusion, allowing parameters like blood flow to be found via mathematical modelling (Ferré et al. 2013). Scans for this technique are typically 3-5 minutes. Recent work has shown promising results using ASL to detect disruptions in the blood-brain barrier in animal models (Dickie et al. 2019; Ohene et al. 2021).

The technique DCE was chosen specifically for its ability to quantify a measure of permeability, rather than the other perfusion-related parameters, as well as for its common use in clinical studies.

Chapter 2

Background

2.1 MRI Physics

2.1.1 Basics

The fundamental principle behind magnetic resonance imaging is utilizing the intrinsic property of subatomic particles: spin. The spin of a nucleus, specifically, is the key to the function of MR imaging. Spin is a term for the inherent angular momentum present in subatomic particles such as neutrons, protons, and electrons. In all elements except 1-hydrogen, nuclei are composed of both neutrons and protons. Depending on its composition, a nucleus might have a spin of zero if the spins of the neutrons and protons cancel each other perfectly, or else might have a non-zero spin. Atoms which have a non-zero charge and non-zero spin—such as protons, electrons, and certain nuclei—will also have a magnetic moment, since moving charges (or a changing electrical field) create a magnetic field. These atoms can be treated as a tiny dipole, like a bar magnet, which can be affected by an externally applied magnetic field.

The type of imaging used in this project was the most common form of MR imaging, that of 1—hydrogen imaging. In a 1-hydrogen atom, the nucleus is composed of a single proton, which, as mentioned previously, has a magnetic moment. The electron can be disregarded in this context, and hydrogen atoms can be treated as solitary protons. Like a bar magnet, protons will have a tendency to align with an external magnetic field. However, this alignment is not completely stationary—though the proton’s magnetic moment will move to align with the magnetic field, it will do so with a precession around a field vector, much like how a spinning top wobbles in a circular motion around the gravitational field vector. An aligned proton precesses at a certain frequency, depending on the strength of the applied magnetic field, and is called the Larmor frequency. The Larmor frequency adheres to the following equation:

$$\omega_0 = \gamma B_0$$

where ω_0 is the Larmor frequency in MHz, γ is the gyromagnetic ratio of the proton or other nucleus in MHz/Tesla, which is the ratio of magnetic momentum to angular momentum of a particle, and B_0 is the applied magnetic field in Tesla.

The Larmor frequency is a very important characteristic of the protons in a magnetic field, as it is used to acquire the signal required for MR imaging. The generation of MR signal starts off by perturbing a proton from its alignment. Perturbing the proton is done by applying another magnetic field, but this time it is not a time-stationary field like the first. Instead, it is an alternating field, oscillating at the Larmor frequency. This field is referred to as the B_1 field. Because it is oscillating at the same frequency that the proton is precessing at, there is a very efficient transfer of energy that would not be possible if they were different frequencies. This oscillating field tilts the proton from its alignment, then when it is turned off, the proton relaxes back into alignment. When it relaxes, it releases the energy which kept it misaligned, and this energy is released as an oscillating magnetic field itself.

There are two distinct properties that become evident during the excitement and subsequent relaxation of protons during MR imaging. These are the two magnetization mechanisms: longitudinal and transverse magnetization. Longitudinal magnetization is magnetization in the direction of the B_0 field, while transverse magnetization is that in the plane perpendicular to the B_0 field. As the protons are tilted out of alignment, their collective longitudinal magnetization is reduced, and their transverse magnetization increases. Then, when the B_1 field is removed, the protons re-align and longitudinal magnetization is restored. This is termed T1 relaxation. However, there is a second form of magnetization relaxation, called T2 relaxation. This relaxation mechanism concerns the loss of phase coherence of spins in the transverse plane that occurs after the protons have been tilted and after the RF pulse is discontinued. This occurs because of small differences in local magnetic fields (i.e. atomic level) for different protons. From influences such as the magnetic moments of nearby atoms each proton's Larmor frequency will be slightly different. Since there is a spectrum of frequencies at which the protons are precessing, though their phases are the same at the time of excitation, they will diverge until the spins are completely out of sync, and no net transverse magnetization remains. Both T1 and T2 properties are important for characterizing tissues with MR imaging.

The descriptions above concern a nuclear magnetic resonance (NMR) experiment yet are still important in MR image contrast mechanisms. But to spatial

localize information and present it as an image, the application of three orthogonal magnetic field gradients is needed. Localization is thus achieved by setting spatial gradients in the magnetic field, such that each voxel location along one direction has a unique magnetic field value. This value is common to all voxels within the same “slice.” From the unique B value, the protons in this location will have a unique Larmor frequency, which can be excited by an applied radiofrequency (RF) pulse at that Larmor frequency, without exciting protons in other slices. This allows for protons to be selected based on spatial location.

Within a selected slice, there are still two dimensions that must be separated to acquire an image. This is done by encoding one direction again with frequency, and the other direction with phase. Frequency encoding is done again by applying a magnetic field gradient across one dimension within the slice. Phase encoding involves turning gradients on and off at specific timing to alter the phase of the precessing protons according to their location.

2.1.2 Dynamic Contrast Enhanced MRI

Dynamic Contrast Enhanced MRI (DCE-MRI) is an application which involves injecting a bolus of contrast agent intravenously and taking a series of images to track the path of the bolus. For the images in this research project, the contrast agent used was gadolinium (Gd^{3+}) based. The Gd is rendered non-toxic, yet still able to interact with water protons and thus enhance their relaxivity, through binding with a chelate. Gd is a paramagnetic T1 contrast agent. The way in which it modulates contrast is that it shortens the T1 relaxation time of protons in its local vicinity, the amount of which is dependent on the concentration of the agent in that location. In the appropriate scan, such as a T1-weighted gradient echo (GRE) MRI scan this results in enhancement of the signal as the contrast agent enters and accumulates. The concentration of the agent can be calculated based on the enhancement of the signal according to the following equations:

$$\frac{1}{T_1} = \frac{1}{T_{10}} + R_1 C_t \qquad \frac{1}{T_2} = \frac{1}{T_{20}} + R_2 C_t$$

R_1 and R_2 are the T1 and T2 relaxivities, respectively. $R_1 = 4.5s^{-1}mM^{-1}$, $R_2 = 5.5s^{-1}mM^{-1}$ at 21°C and 1.5T (Tofts et al. 1993). T_{20}^* and T_{10} are the initial values of T_2^* and T_1 , respectively (pre-contrast injection).

2.2 Pharmacokinetic Modelling of Microvascular Permeability

There exist heuristic models which give qualitative results on DCE-MRI (Yuan et al. 2012), as well as semi-quantitative models (Chassidim et al. 2013), which can give indications of higher leakage through vasculature using comparison with healthy tissue. Quantitative measurements of permeability, however, can be achieved using pharmacokinetic modelling of the contrast agent coursing through the body and provides numerical values for physiological properties of vasculature, such as blood volume, blood flow, and permeability. This project is concerned with comparing the use of four different pharmacokinetic models for the quantification of permeability of vasculature.

All the models investigated in this thesis follow a similar form: all are based on a two-compartment model of the vascular space and surrounding extracellular-extravascular space. Additionally, they all treat the passage of tracer through the capillary walls as a convolution of an input function and an impulse response function of the tissue. The input function is the concentration-time curve within the vasculature, which is found using the signal within the supplying artery, in this case the middle cerebral artery (MCA). It should be noted that the permeability is not directly quantified in any of these models, however, closely related parameters are quantified. Permeability through a membrane, which is modeled based on Fick's law, requires knowledge of the surface area of the membrane. It is not possible to know or measure the surface area of brain capillaries. Hence the loosely referred to term of 'permeability' really means permeability - surface area product.

The models investigated were the Two-Compartment Exchange Model (2XCM), the Uptake model, the Tofts model, and the modified Tofts model. A previous study has investigated these models in cervical tumours to determine which model was most appropriate (Donaldson et al. 2010). Their results indicated that the 2XCM and Uptake models were superior to the Tofts models. However, due to the highly vascularized and hyperpermeable nature of tumours, the assumptions which are appropriate in that environment may be different from those in the highly regulated environment of the brain microvasculature.

One benefit of the less general models is that they have less parameters to fit, which leads to less computation time. However, making inaccurate assumptions will lead to a less accurate fit. For the aforementioned Donaldson 2010 study, tumours are typically highly vascular, with highly permeable vasculature, which is a large contrast to vasculature in the brain, especially that which contains the blood-brain barrier. Therefore, the superior model for pharmacokinetic modelling in the brain may very well be different from that in a tumour.

2.2.1 Two-Compartment Exchange Model

The two-compartment exchange model is a four-parameter model (Brix et al. 2004). This model, as illustrated in (Fig. 2.1), consists of two compartments: the vascular space and the extracellular-extravascular space.

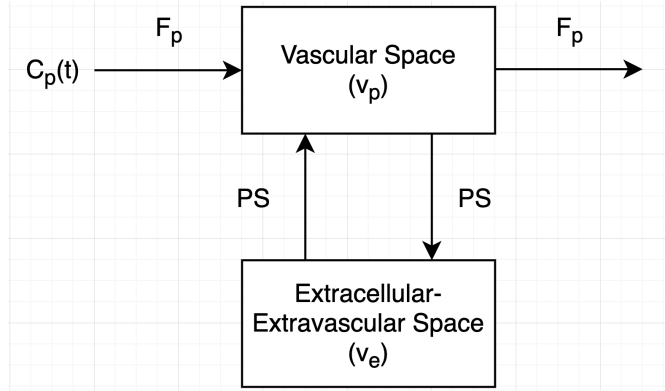


FIGURE 2.1: Two-Compartment Exchange Model Schematic.

The parameters it uses are F_p , which is the plasma perfusion, related to the rate at which the contrast agent is delivered to the vascular space, and PS , the permeability-surface area product of the capillary walls, respectively. P is permeability, described as the outflux of tracer per unit wall area, per unit concentration locally. S is the surface area of the walls. These two values can't be separated, nonetheless they still provide valuable quantification of the microvasculature.

This general model can be described with the following equation :

$$C_t(t) = F_p C_p(t) * R_{2CXM}(t)$$

where $C_t(t)$ is the concentration-time curve of tracer in the voxel, $C_p(t)$ is the concentration-time curve of tracer in the plasma space, $*$ is the convolution operator, and $R_{2CXM}(t)$ is the impulse response function of the tissue:

$$R_{2CXM}(t) = Ae^{-\alpha t} + (1 - A)e^{-\beta t}$$

The model four parameters (F_p , A , α , and β . C_t) are determined from the signal-time course in each voxel, while $C_p(t)$ is estimated from the signal in the supplying artery, called the arterial input function (AIF). A , α , and β are related to the transfer constants, k_{01} , k_{12} and k_{21} , which are in turn related to the permeability-surface area product, PS , the vascular space, v_p , and the EES, v_e .

$$k_{01} = A(\alpha - \beta) + \beta; k_{12} = \frac{\alpha\beta}{k_{01}}; k_{21} = \alpha + \beta - k_{12} - k_{01}$$

$$PS = k_{21}v_p; v_p = \frac{F_p}{k_{01}}; v_e = \frac{PS}{k_{12}}$$

2.2.2 Uptake Model

The Uptake model has the closest form to the 2XCM general model. It is appropriate for situations where acquisition time is limited, and so the EES has not filled up with tracer to a level where the outflux is significant (Bazelaire et al. 2005). From this, the transfer constant of tracer from the EES back into the plasma, k_{12} , is assumed to be zero. It uses the same equation for $C_t(t)$, but with a different impulse response function, $R_{uptake}(t)$.

The impulse response has the following form:

$$R_{uptake}(t) = (1 - B)e^{-zt} + B$$

z is the plasma mean transit time (MTT), the average time tracer spends in the plasma compartment. B is related to the same transfer constants as in 2XCM, with the exception of k_{12} which, as mentioned before, is ignored. From the 2XCM concentration equation, this model also uses the plasma perfusion, F_p , making this a three-parameter model.

$$PS = \frac{BF_p}{1 - B}; v_p = \frac{F_p z}{1 - B}$$

$$B = \frac{k_{21}}{k_{01} + k_{21}}$$

2.2.3 The Tofts Model

The Tofts model, as well as its variation called the modified Tofts model, assumes a two-compartment model, as shown in (Fig. 2.2), but it models different parameters than the 2XCM and Uptake models (Tofts and Kermode 1991; Tofts et al. 1995; Tofts et al. 1999). It also makes the assumption that the plasma mean transit time (MTT) is negligible.

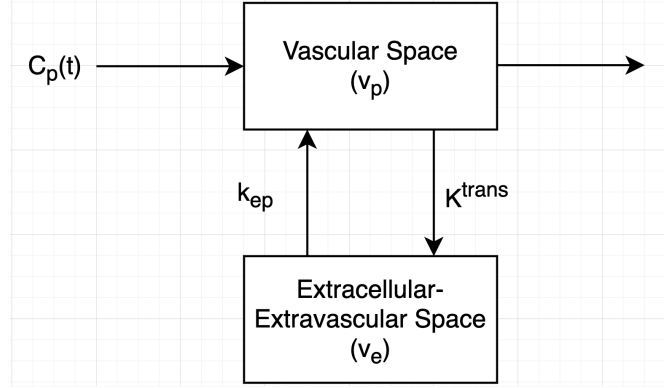


FIGURE 2.2: Tofts Model Schematic.

In the schematic it is noted that parameters in both Tofts models use are K^{trans} and k_{ep} . These denote the influx and outflux mass transfer rates– i.e. the flow of tracer from plasma to EES, and back. They have the following relationship:

$$k_{ep} = \frac{K^{\text{trans}}}{v_e}$$

This relationship reduces the Tofts model to a two-parameter model, with the following concentration-time curve and impulse response function:

$$C_t(t) = C_p(t) * R_{\text{Tofts}}(t) \quad R_{\text{Tofts}}(t) = K^{\text{trans}} e^{-\frac{K^{\text{trans}} t}{v_e}}$$

In the Tofts model, the contribution of signal from the tracer within the plasma space is assumed to be negligible. The parameter K^{trans} physiologically represents a combination of F_p and PS from the 2CXM (Tofts et al. 1999). This results in a parameter with varying meaning: in low-permeability tissue, K^{trans} reflects permeability, and in high-permeability tissue, K^{trans} reflects blood flow (Essig et al. 2013).

2.2.4 The Modified Tofts Model

The modified Tofts model simply has the change that the contribution of the tracer within the plasma space is not negligible, so the concentration-time curve has the added parameter of v_p , making this a three-parameter model (Tofts 1997).

$$C_t(t) = v_p C_p(t) + C_p(t) * R_{\text{Tofts}}(t)$$

Chapter 3

Methods

3.1 Subjects

The data of eight healthy subjects between the ages of 19 to 31, mean age of 22, were used for this analysis. Six of these subjects were female, two were male. Six subjects returned for repeat scans eight weeks later (four female, two male), so a total of fourteen scan sets were used for this analysis. The study was approved by the Hamilton Integrated Research Ethics Board (<http://HiREB.ca>), with Dr. Benicio Frey as the principle investigator.

3.2 Scan Parameters

The BBB permeability was assessed using dynamic contrast enhanced MRI in combination with a geometrically matched T1-map. The pre-contrast T1-map is essential for all parametric modelled dceMRI scans (Tofts et al. 1995). The T1map was determined through a combination of T1 weighted (T1W), proton-density weighted (PDW) and B1+ maps. Volunteers, before the scanning procedure, had a 20 gauge catheter inserted into the left antecubital vein. This was hooked up to a power injector pump that slowly delivered saline to keep the line patent.

The T1W scan was an ultrafast 3D sagittal BRAVO whole brain scan (flip angle 12, TR = 7.908 ms, TE = 3.06 ms, TI = 450 ms, field of view (FOV) = 24cm, 256x256, pixel bandwidth = 244.1410Hz/pixel, 188 slices) while the PD scan was a 3D sagittal fast SPOiled Gradient Recalled Echo (fSPGR) sequence (flip angle 4, TR = 7.908 ms, TE = 3.06 ms, FOV = 24cm, 240x240, pixel bandwidth = 260.4170Hz/pixel, 188 slices). A B1+ field map was also acquired for field corrections and was acquired using the GE field mapping tool built into the scanner. Subsequently, subjects were given an intravenous injection of gadobutrol, a macrocyclic non-ionic gadolinium-based contrast agent, (0.1 mM/kg body weight, Gadovist, Bayer, Leverkusen Germany), while rapidly scanning the whole brain

using DCE-MRI imaging. Injection of Gadovist was immediately followed with injection of 20cc of saline (0.9% w/v) flush. Injection was done with a MRI compatible Medrad Spectris Solaris EP Power injector (Bayer) at 3cc/sec. This last scan was an optimized T1-weighted 3D protocol (GRE scan, flip angle 30, TR=3.8 ms, TE=1.2 ms, FOV= 24cm, 192x192matrix, receiver bandwidth (rbw) = 62.5kHz, 34 slices, ASSET factor =2, 40 temporal phases, 1.25mm x 1.25mm x 7.1mm voxel size). The temporal resolution for whole brain acquisition was 11.3 seconds.

3.3 Pre-processing

The first step for pre-processing was to perform registration of the brains, to remove any motion that may have occurred during the scan and make sure each voxel lined up with the correct location. Additionally, the brains were registered to the standard MNI 152 1mm T1W template so that the brains of different patients could be compared. The application used for this was FSL (Smith et al. 2004), using their FLIRT function (FMRIB's Linear Image Registration Tool) with trilinear interpolation and 12 degrees of freedom (Jenkinson and Smith 2001; Jenkinson et al. 2002).

The proton density weighted (PDW) image, the B1+ map, and the DCE images were first registered to the T1 weighted anatomical image, to remove any motion of the patient between or during scans. The T1 weighted images were then registered to the MNI 152 1mm T1W template, and the transformation matrix of this registration was applied to the PDW image, the B1+ map, and the DCE image so that all scans were registered to the MNI template. The new T1W and PDW images were then used to create a map of the T1 values in the patient's brain, with the B1+ map used for magnetic field correction. This was done using an in-house Matlab script written by Kim Desmond.

3.4 Processing

The entirety of the pharmacokinetic modelling was done using Matlab (R2020b), with functions from the Optimization Toolbox.

3.4.1 Signal to Concentration

Using the T1 map of the brain, the concentration of gadolinium present in each voxel was calculated for each image in the DCE scan using the following equation (Wehrli et al. 1990):

$$S(C_t) = GPD e^{-TE(T_{20}^{*-1} + R_2 C_t)} \sin \theta \frac{1 - e^{-TR(T_{10}^{-1} + R_1 C_t)}}{1 - \cos \theta e^{-TR(T_{10}^{-1} + R_1 C_t)}}$$

where G is the gain and PD is the proton density within the voxel. R_1 and R_2 are the relaxivities of the contrast agent, Gadovist, which are 5.0 and 7.1 L mmol⁻¹ s⁻¹ in plasma at 37 ° C and 3T (Rohrer et al. 2005). T_{10} is the initial T1 value, before any contrast was injected, found from the T1 map that was generated.

This relationship can be simplified by normalizing the time intensity to the initial signal before the injection, when $C_t = 0$, $S(0)$, to achieve the following relationship:

$$\frac{S(C_t)}{S(0)} = \frac{1}{C} e^{-TER_2 C_t} \sin \theta \frac{1 - e^{-TR(T_{10}^{-1} + R_1 C_t)}}{1 - \cos \theta e^{-TR(T_{10}^{-1} + R_1 C_t)}}$$

where

$$C = \sin \theta \frac{1 - e^{-TR/T_{10}}}{1 - \cos \theta e^{-TR/T_{10}}}$$

With these equations, the normalized signal in each voxel was calculated for each time point, and the concentration of contrast agent present was subsequently determined.

3.4.2 Anatomical Regions of Interest

Using manually drawn masks of regions of interests in the MNI template, the average concentration-time curve was found for each ROI. The regions of interest included: amygdala, head of the caudate nucleus, thalamus, putamen, pons, cerebellum, hippocampus, and posterior pituitary, as shown in figures 3.1 to 3.4. Due to its small size, an individual posterior pituitary mask was created manually for each patient, while the other ROIs were made based on the MNI template and applied to all patients. The hippocampus, amygdala, putamen, caudate, cerebellum, thalamus are regions of the brain in which structural differences have been found between healthy and bipolar subjects (Brambilla et al. 2005), and are therefore areas of interest for future investigations of subtle BBB dysfunction.

3.4.3 Arterial Input Function

For the methods that were compared, the parameters of microvascular permeability were found from a model based on a convolution of an arterial input function

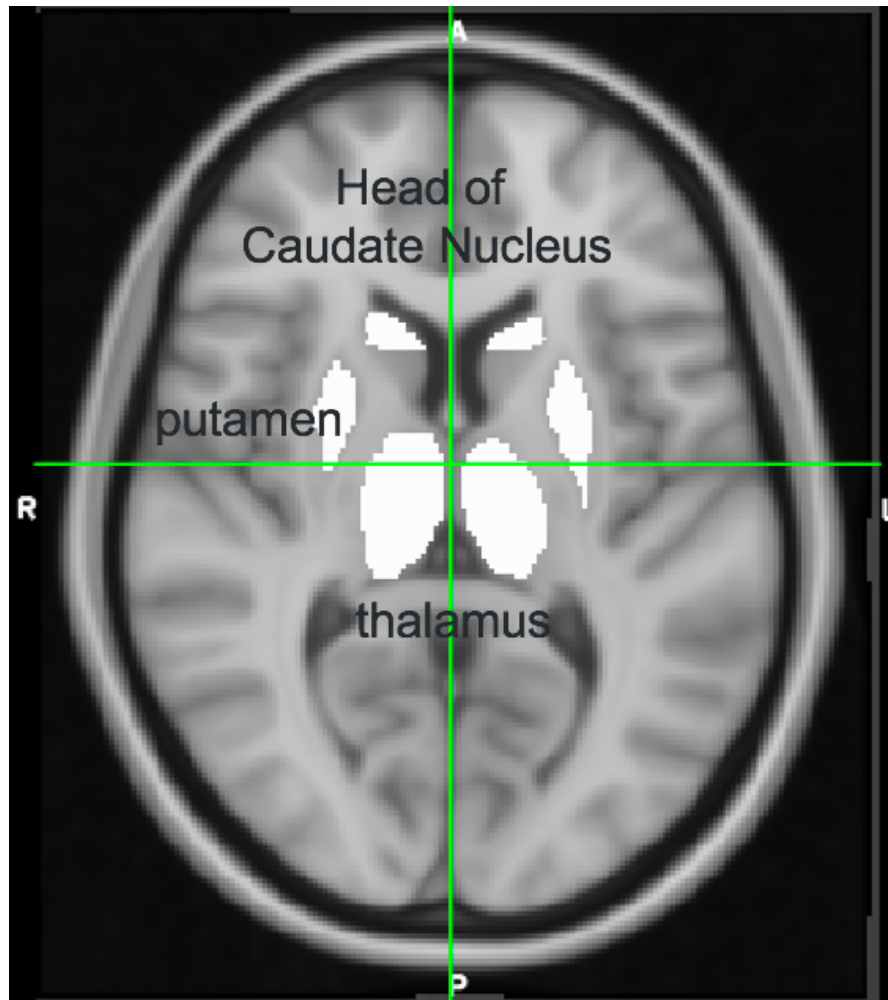


FIGURE 3.1: Bilateral regions of interest, head of caudate nucleus, putamen, and thalamus.

(AIF) with the method's unique impulse response function. Although different ROIs may have different supplying arteries, it was assumed that the AIF in each ROI would have the same shape and timing, so the AIF found in the middle cerebral artery (MCA) was used for all ROIs. A large mask was drawn around the MCA in the MNI template, with large margins surrounding the artery, to account for any error in registration, so that the MCA would be within the ROI. A Matlab program was written to take the voxels within the MCA ROI with the highest signal enhancement in the DCE image (greater than five times the average enhancement in the ROI), assuming those were voxels within the artery. The contrast agent concentration of those voxels was then calculated in the same way as described previously. The average of the concentration-time curve in those

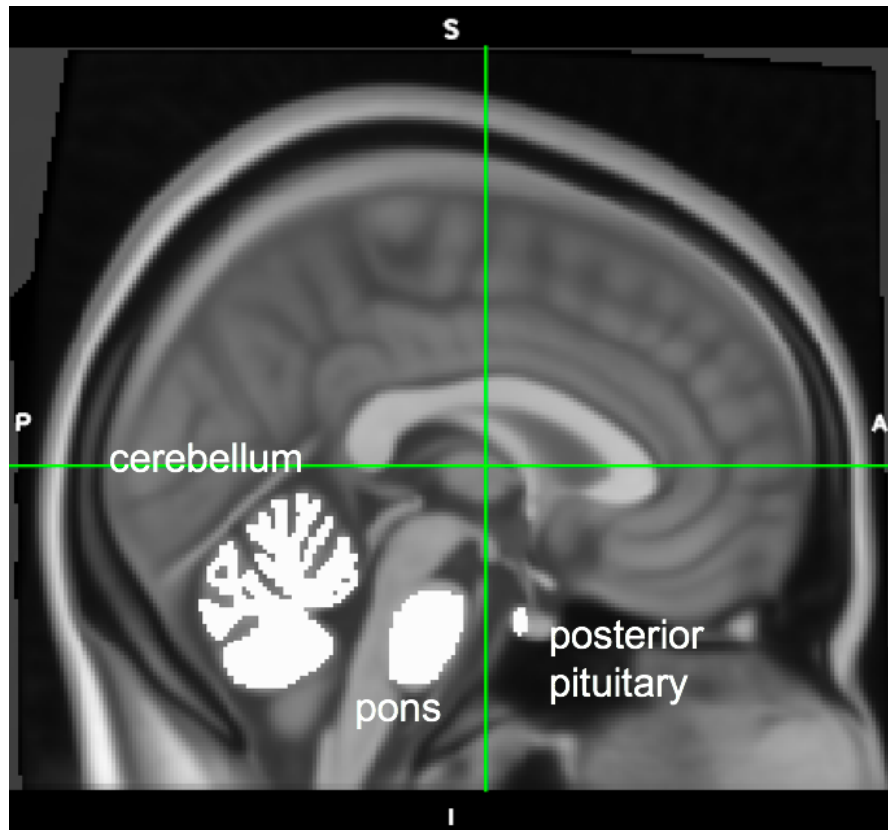


FIGURE 3.2: Midline regions of interest, cerebellum, posterior pituitary, and pons.

voxels was subsequently used as the AIF. See figure 3.5 for example.

3.4.4 Model Fitting

After finding the concentration time curve, the data was fitted using Matlab's `lsqcurvefit` function. It used each model's individual concentration equation and impulse response function as the fitting function and optimized the fit for each data set. Limits were placed on the fitting parameters to keep them positive.

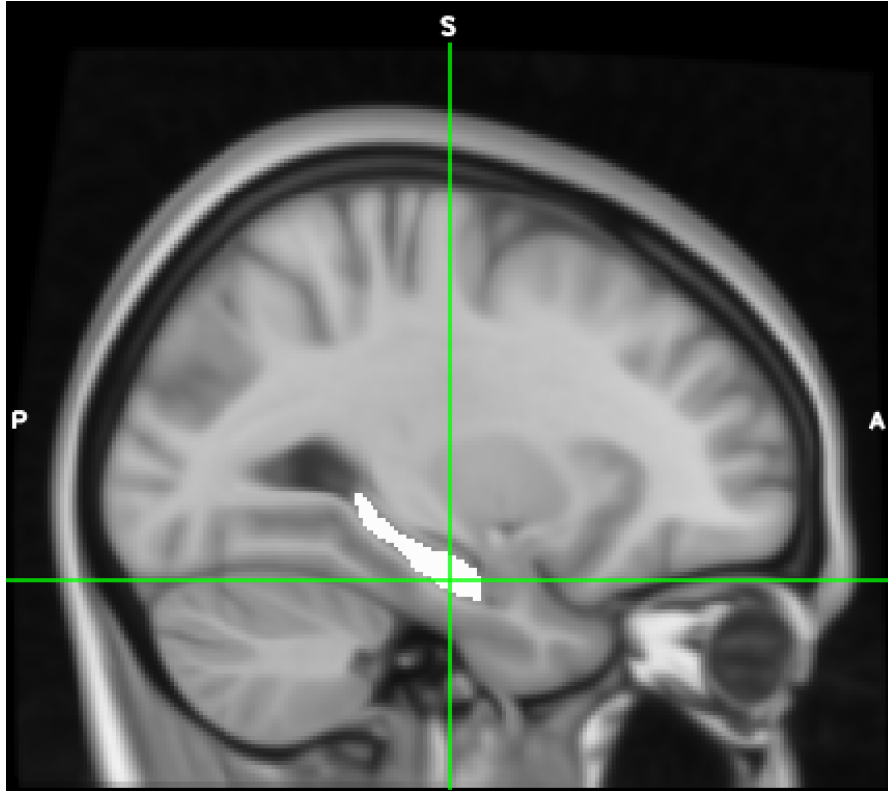


FIGURE 3.3: Right hippocampus region of interest.

3.5 Statistical Comparison of Models

After the data was fitted with all four models, the coefficient of determination, R^2 , was found using the following formula:

$$R^2 = 1 - \frac{SS_{res}}{SS_{tot}}$$

SS_{tot} is the total sum of squares, which is proportional to the variance of the data, and SS_{res} is the residual sum of squares, which is a measure of the difference between the actual value (y_i) and the fitted value (f_i). They are found using these equations:

$$SS_{tot} = \sum_i (y_i - \bar{y})^2$$

$$SS_{res} = \sum_i (y_i - f_i)^2$$

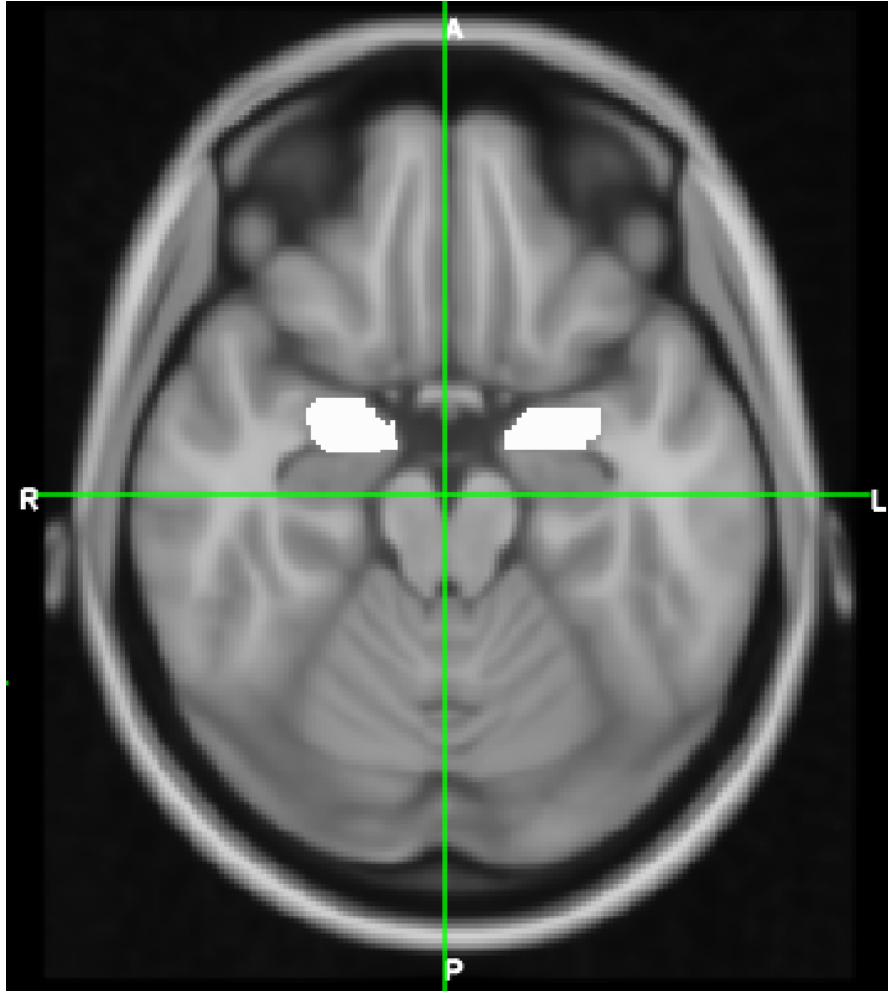


FIGURE 3.4: Amygdala regions of interest.

This value give a measure of the error between the fit and the data, with a R^2 value of 1 being a perfect fit with no deviation from the real data. Negative values of R^2 are possible and represent a fit that is worse than a horizontal line going through the data at the mean y value.

3.6 Considerations

There were certain issues and decisions which arose that had the potential to compromise the accuracy of the permeability analysis results. In the interest of optimizing the results, these issues were investigated to see if they did indeed have an effect on the results, and determine what solution might mitigate those effects.

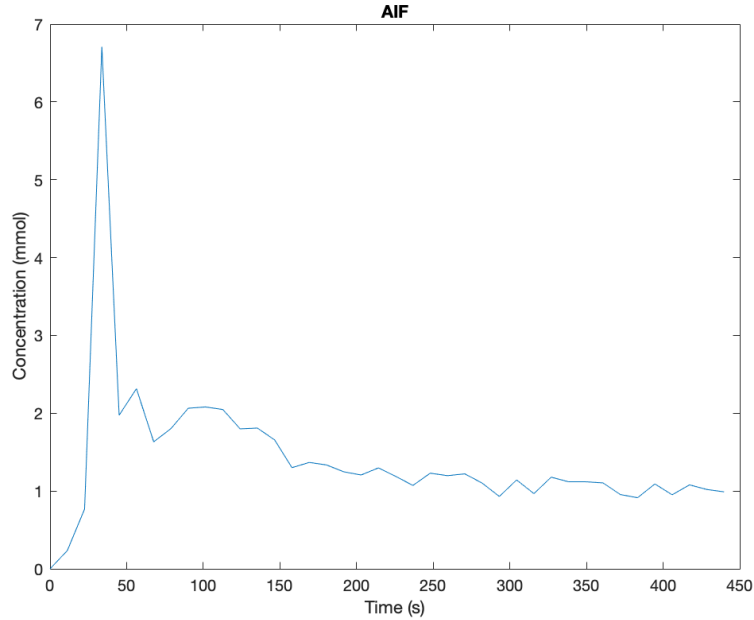


FIGURE 3.5: Example arterial input function from subject 8173.

3.6.1 Signal vs. Concentration

As mentioned previously, in order to find the concentration in each voxel, the following relationship between signal and concentration was used:

$$\frac{S(C_t)}{S(0)} = \frac{1}{C} e^{-TER_2 C_t} \sin \theta \frac{1 - e^{-TR(T_{10}^{-1} + R_1 C_t)}}{1 - \cos \theta e^{-TR(T_{10}^{-1} + R_1 C_t)}}$$

However, the relationship of signal and concentration is not one-to-one, that is at multiple points the function has two possible concentration values for the signal, as shown in 3.6. Near the peak of this curve the calculation of the incorrect concentration would have less error, but further away from the peak on either side would have much more error. Algorithms to solve for the concentration value using this equation would not tend to discriminate between the two possible values, which would lead to significant error in the concentration curve. To avoid this, limits were placed on the signal-concentration function, with the concentration going from 0 to the concentration corresponding to the maximum signal (which was calculated for each voxel based on the T_{10} value). This prevented high concentration values from being accidentally calculated when low concentration values are expected (like at the beginning or end of the concentration-time curve).

Even with this modification, there was still the possibility that concentrations beyond the peak would be present in the brain, and would not be dealt with appropriately with these constraints. The highest concentration one would expect to encounter would be in the plasma concentration, or the AIF, however these concentration values did not approach the peak-signal concentration values, and so no special measures needed to be taken. Additionally, if the concentration in a voxel had reached the peak-signal value and surpassed it, the signal would have showed a dip in the curve rather than reaching a singular peak- in other words, would have had two peaks. This shape was never seen in the signal curves, so it seems that this problem is not one of consideration.

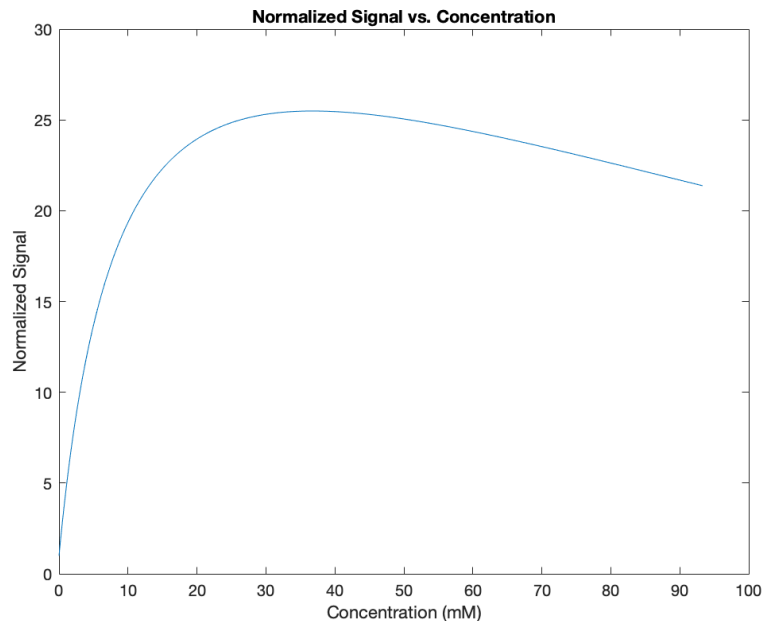


FIGURE 3.6: Signal vs. Tracer Concentration, with a T10 of 0.911 s, a typical white matter value at 3T (Dieringer et al. 2014).

3.6.2 Registration Interpolation Methods

The FSL software package gives the option of choosing the interpolation method when registering images. These options are sinc, trilinear, and nearest neighbour. The trilinear interpolation method was chosen due to some effects sinc interpolation was having on certain pixels. Sinc interpolation is often used due to its non-linearity, which results in smoother registered images. However, this also allows for values outside the original range to be present in the registered images, whereas this never occurs with trilinear interpolation. This was seen when the

DCE images were registered to the MNI template, where certain voxels had much lower or even negative signal values. The issue with this arose when concentration curves for voxel-by-voxel analysis were being calculated, since the signal is normalized to the first time point. Occasionally a concentration curve had an abnormally high peak due to the initial signal having been interpolated to a much smaller value, and when the initial signal had a negative value, the curves had been completely inverted. This was a rare occurrence, which mainly seemed to happen near sharp contrast areas (i.e. high spatial frequency boundaries) like around bone, but in an effort to maximize accuracy the trilinear method was used instead.

3.6.3 Order of Concentration Calculation

When calculating microvascular permeability values over ROIs, the average concentration-time curve was fitted with whatever model was being investigated. This leaves the opportunity for choice of when to take this average- one can either find the concentration curve for each voxel using their individual T10 values and take the average of the concentration curves, or alternatively the average T10 and signal can be found first and then used to solve for a single concentration curve. It was noted in (Donaldson et al. 2010) that their procedure did the former, taking the average T10 value of the ROI encompassing the tumour and the average signal to calculate concentration. However, since the relationship between signal and concentration is not linear with respect to T10, taking the average before the concentration calculation might produce inaccurate results- whether these differences are significant is another question.

Both methods were tested in the posterior pituitary to determine if they had an effect (see figures 3.7, 3.8, 3.9, 3.10). Method 1 focused on finding the average after the concentration calculation, while the second method determined it before. As shown in the figures, a difference between the methods was noted. Based on the literature it was assumed the first method should be the more accurate of the two, so it was used for this project.

Another notable comment is that within an ROI, even one which appears uniform, the individual voxels within the ROI will have different composition of both plasma space and extracellular-extravascular space, as described by all the models. The assumption that the average signal and T10 would be representative of the average concentration throughout an ROI would be less appropriate in tissue with high variability of T10 within- for example, highly inhomogeneous tissue like that with a high percentage of microvasculature. It stands to reason that these sorts of tissue, like those found in tumours, would be ill-suited to the second method. Tests comparing the two methods on different tissues would be beneficial to see the

extent the error from averaging too soon propagates into the final concentration values.

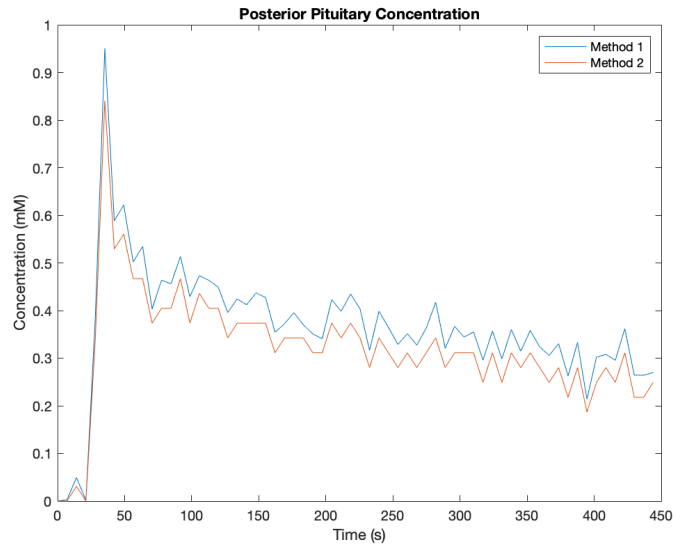


FIGURE 3.7: Concentration curves in posterior pituitary of subject 8126 using different orders of averaging (1: average after concentration curves are found, 2: average before concentration curve is found.)

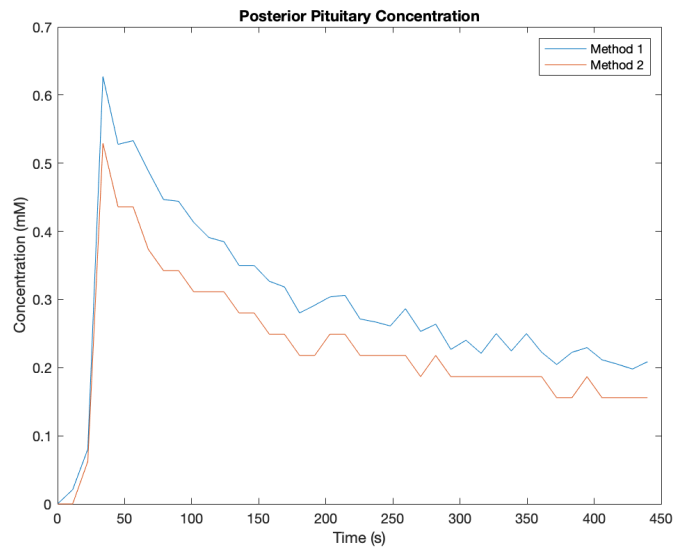


FIGURE 3.8: Concentration curves in posterior pituitary of subject 8173 using different orders of averaging.

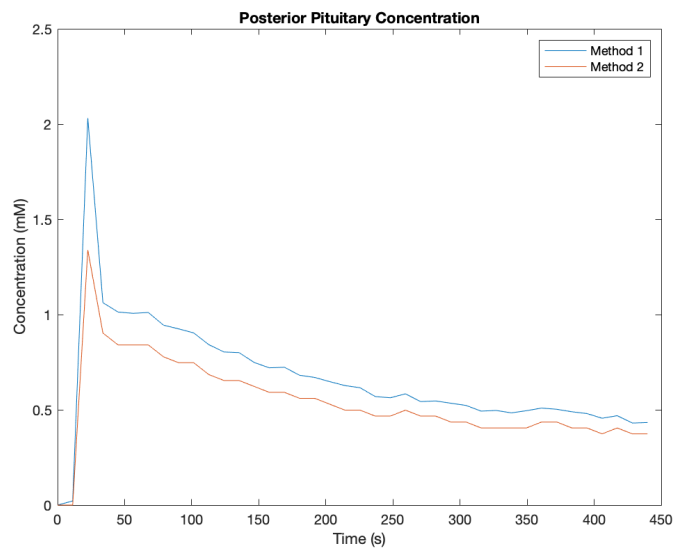


FIGURE 3.9: Concentration curves in posterior pituitary of subject 8239 using different orders of averaging.

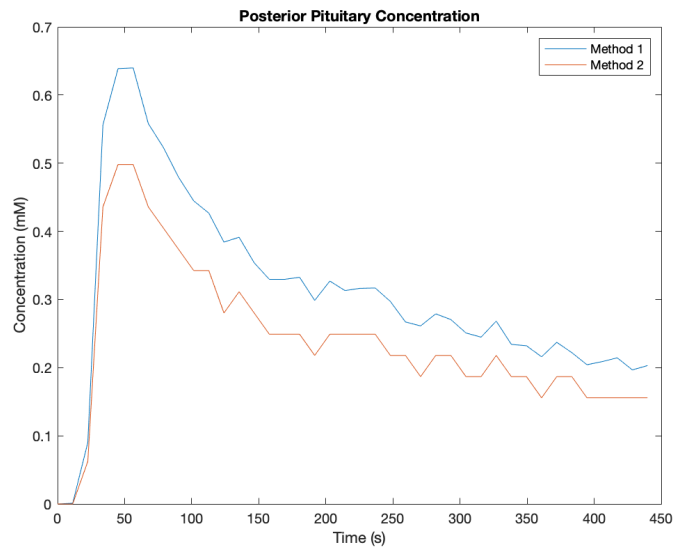


FIGURE 3.10: Concentration curves in posterior pituitary of subject 8264 using different orders of averaging.)

Chapter 4

Results

Nine subjects underwent scanning, though one was removed from the data set due to an incidental finding. Six subjects were scanned twice. All remaining data was usable and no issues arose in running all pre-processing and processing automatically after the final version of the code had been written.

4.1 Tabular Results

It is difficult to compare absolute metrics of microvascular permeability for each model since there is no 'gold standard'. The only comparisons that can be made are based on model fit error and whether permeability measures seemed to adequately be lower than that of the posterior pituitary, which is void of a BBB. Furthermore, because of the lack of a BBB in the posterior pituitary the models should fit best there due to the potential higher contrast difference between pre and post contrast injection. Table 4.1 shows the mean R^2 values and standard deviation of each model for each ROI. The posterior pituitary had the highest overall R^2 values, and the lowest standard deviation.

Below are the mean parameter values and their standard deviation for each ROI, with the associated model in subscript. The same parameters are next to each other for easy comparison- it is evident that different models may calculate very different values for the same parameter, as well as a high variability between subjects. Raw data for each scan can be found in Appendix B. Table A2.1 provides an index of what each parameter means and its units.

TABLE 4.1: Table of mean R^2 for each model in each ROI.

ROI	R^2_{Tofts}	R^2_{modTofts}	R^2_{2CXM}	R^2_{Uptake}
Posterior Pituitary	0.88 ± 0.09	0.91 ± 0.09	0.93 ± 0.08	0.91 ± 0.07
Pons	0.55 ± 0.2	0.71 ± 0.21	0.66 ± 0.21	0.69 ± 0.21
Cerebellum	0.73 ± 0.17	0.8 ± 0.15	0.61 ± 0.39	0.8 ± 0.16
Putamen L	0.38 ± 0.31	0.53 ± 0.24	0.39 ± 0.63	0.52 ± 0.26
Putamen R	0.53 ± 0.3	0.63 ± 0.28	0.56 ± 0.27	0.59 ± 0.27
Amygdala L	0.47 ± 0.35	0.59 ± 0.29	0.39 ± 0.56	0.57 ± 0.32
Amygdala R	0.51 ± 0.35	0.63 ± 0.33	0.42 ± 0.41	0.59 ± 0.34
Thalamus L	0.57 ± 0.24	0.66 ± 0.21	0.64 ± 0.19	0.67 ± 0.2
Thalamus R	0.63 ± 0.22	0.7 ± 0.21	0.66 ± 0.21	0.7 ± 0.19
H of C N L	0.52 ± 0.25	0.62 ± 0.2	0.53 ± 0.3	0.6 ± 0.21
H of C N R	0.57 ± 0.25	0.66 ± 0.23	0.56 ± 0.33	0.64 ± 0.24
Hippocampus L	0.65 ± 0.22	0.73 ± 0.19	0.6 ± 0.44	0.74 ± 0.17
Hippocampus R	0.78 ± 0.12	0.84 ± 0.09	0.76 ± 0.17	0.82 ± 0.08

TABLE 4.2: Index for Parameter Units

Parameter	Description	Units
K^{trans}	Volume Transfer Rate	/s
PS	Permeability-Surface Area Product	mM/s
v_e	EES Volume Fraction	Unitless
v_p	Plasma Volume Fraction	Unitless
F_p	Plasma Perfusion	mM/s
z	Plasma Mean Transit Time	s

4.2 Results Figures

The figures below are some examples of the fitted data in different subjects and regions. Figure 4.1 depicts a concentration curve where the models had indistinguishable fits, and their R^2 values were all 0.975. This ROI was in the posterior pituitary gland. Figures 4.2, 4.3 and 4.4 show the concentration curve in the right amygdala of three different subjects, which all had slight differences between the fits of the models- however with figure 4.4 having a very low R^2 across all models (between 0.004 and 0.04). Figure 4.5 shows the left putamen of a fifth subject, with large differences between the four models. Note the low concentration values and high degree of noise.

TABLE 4.3: Table of mean permeability parameters for each ROI.

ROI	$K^{\text{trans}}_{\text{Tofts}}$	$K^{\text{trans}}_{\text{modTofts}}$	PS _{2CXM}	PS _{Uptake}
Posterior Pituitary	0.00971 ± 0.00593	0.0062 ± 0.0048	0.001618 ± 0.002176	0.000161 ± 0.000147
Pons	0.00107 ± 0.0005	0.00038 ± 0.00039	0.000072 ± 0.000115	0.000022 ± 0.000019
Cerebellum	0.00079 ± 0.00041	0.00031 ± 0.00021	0.000029 ± 0.000092	0.000013 ± 0.00001
Putamen L	0.00076 ± 0.00044	0.00044 ± 0.00043	0.000045 ± 0.000077	0.000019 ± 0.00002
Putamen R	0.00074 ± 0.00042	0.00025 ± 0.0002	0.000026 ± 0.000053	0.000013 ± 0.000012
Amygdala L	0.00112 ± 0.00123	0.00046 ± 0.00055	0.000023 ± 0.000062	0.000013 ± 0.000012
Amygdala R	0.00082 ± 0.00066	0.00024 ± 0.00028	0.000019 ± 0.000049	0.000011 ± 0.000009
Thalamus L	0.00087 ± 0.00039	0.00035 ± 0.00025	0.000023 ± 0.000044	0.00002 ± 0.000021
Thalamus R	0.00086 ± 0.00042	0.00033 ± 0.00026	0.00002 ± 0.000042	0.000015 ± 0.000015
H of C N L	0.00062 ± 0.00038	0.00026 ± 0.00025	0.000075 ± 0.000233	0.00001 ± 0.00001
H of C N R	0.00058 ± 0.00038	0.00019 ± 0.00016	0.000006 ± 0.000017	0.00001 ± 0.000008
Hippocampus L	0.00099 ± 0.00048	0.00037 ± 0.00033	0.000031 ± 0.000081	0.000016 ± 0.000012
Hippocampus R	0.00086 ± 0.00038	0.00036 ± 0.0003	0.00001 ± 0.000028	0.00001 ± 0.000009

TABLE 4.4: Table of mean values of extracellular-extravascular and plasma volume fraction for each ROI.

ROI	V_e, Tofts	$V_e, \text{modTofts}$	$V_e, \text{2CXM}$	$V_p, \text{modTofts}$	$V_p, \text{2CXM}$	V_p, Uptake
Posterior Pituitary	0.2462 ± 0.1328	0.2255 ± 0.1207	0.0998 ± 0.0982	0.0523 ± 0.0627	0.1565 ± 0.0967	0.2072 ± 0.1059
Pons	0.0144 ± 0.0113	0.0127 ± 0.0103	0.007 ± 0.0112	0.0094 ± 0.0059	0.0073 ± 0.0062	0.0087 ± 0.0066
Cerebellum	0.0127 ± 0.0087	0.0116 ± 0.0081	0.0019 ± 0.0049	0.0059 ± 0.0051	0.0086 ± 0.0082	0.0094 ± 0.0069
Putamen L	0.0143 ± 0.0123	0.013 ± 0.0112	0.0072 ± 0.0114	0.0057 ± 0.0052	0.0063 ± 0.0068	0.0083 ± 0.0074
Putamen R	0.0108 ± 0.0085	0.0093 ± 0.0068	0.0029 ± 0.0061	0.0067 ± 0.0059	0.0068 ± 0.0084	0.0053 ± 0.0057
Amygdala L	0.0099 ± 0.0098	0.0089 ± 0.0084	0.0027 ± 0.0078	0.008 ± 0.0119	0.0064 ± 0.0061	0.007 ± 0.007
Amygdala R	0.0081 ± 0.005	0.0073 ± 0.0044	0.0011 ± 0.0029	0.0071 ± 0.0066	0.0042 ± 0.0038	0.0042 ± 0.0033
Thalamus L	0.0158 ± 0.0121	0.0157 ± 0.0123	0.0122 ± 0.034	0.0073 ± 0.005	0.012 ± 0.0083	0.0108 ± 0.0073
Thalamus R	0.0141 ± 0.0109	0.0127 ± 0.0102	0.0048 ± 0.0117	0.0069 ± 0.0062	0.0101 ± 0.01	0.0101 ± 0.0082
H of C N L	0.0093 ± 0.0078	0.0081 ± 0.0065	0.0031 ± 0.0061	0.0052 ± 0.0043	0.0046 ± 0.0042	0.0069 ± 0.0057
H of C N R	0.0082 ± 0.0071	0.0075 ± 0.0061	0.0009 ± 0.0024	0.0049 ± 0.0046	0.0056 ± 0.0067	0.0058 ± 0.0055
Hippocampus L	0.0147 ± 0.0108	0.0132 ± 0.0103	0.0037 ± 0.0078	0.0078 ± 0.0057	0.011 ± 0.0076	0.0112 ± 0.0086
Hippocampus R	0.0118 ± 0.0097	0.0104 ± 0.009	0.0005 ± 0.0016	0.0062 ± 0.0051	0.0095 ± 0.0107	0.0094 ± 0.0089

TABLE 4.5: Table of mean values of plasma perfusion and MTT for each ROI.

ROI	$F_{p, 2CXM}$	$F_{p, Uptake}$	Z_{Uptake}
Posterior Pituitary	0.0107 ± 0.0066	0.0103 ± 0.0063	0.0607 ± 0.0538
Pons	0.0012 ± 0.0006	0.0012 ± 0.0005	0.3615 ± 0.4217
Cerebellum	0.0009 ± 0.0005	0.0008 ± 0.0004	0.2456 ± 0.3343
Putamen L	0.001 ± 0.0005	0.0009 ± 0.0005	0.3468 ± 0.4329
Putamen R	0.0008 ± 0.0004	0.0009 ± 0.0005	0.4843 ± 0.4545
Amygdala L	0.0012 ± 0.0012	0.0011 ± 0.0012	0.3857 ± 0.4209
Amygdala R	0.001 ± 0.0006	0.0009 ± 0.0006	0.4951 ± 0.4611
Thalamus L	0.0009 ± 0.0004	0.0009 ± 0.0003	0.2322 ± 0.3366
Thalamus R	0.001 ± 0.0005	0.0009 ± 0.0004	0.2585 ± 0.363
H of C N L	0.0008 ± 0.0005	0.0007 ± 0.0004	0.2848 ± 0.3922
H of C N R	0.0007 ± 0.0005	0.0006 ± 0.0004	0.3372 ± 0.4361
Hippocampus L	0.0011 ± 0.0005	0.001 ± 0.0005	0.2278 ± 0.3316
Hippocampus R	0.0009 ± 0.0004	0.0009 ± 0.0004	0.2565 ± 0.3333

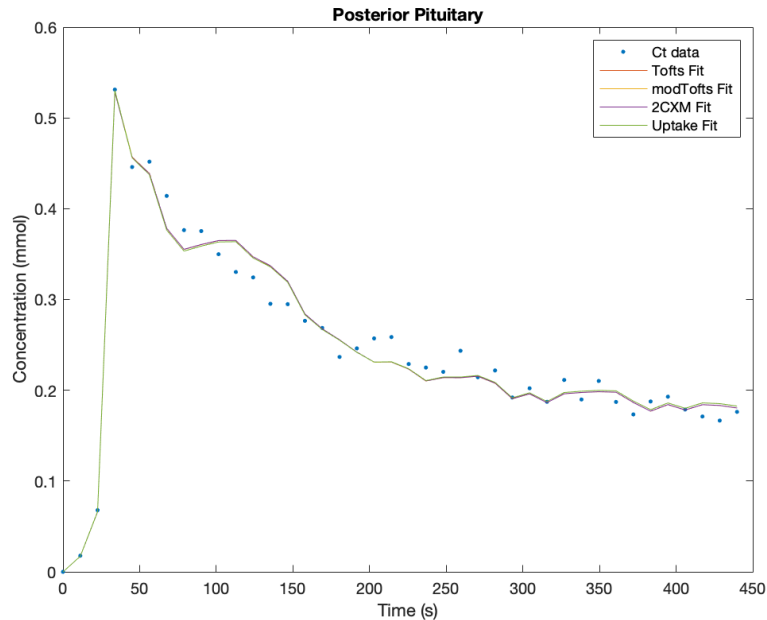


FIGURE 4.1: Concentration-time data within the posterior pituitary of exam 8173.

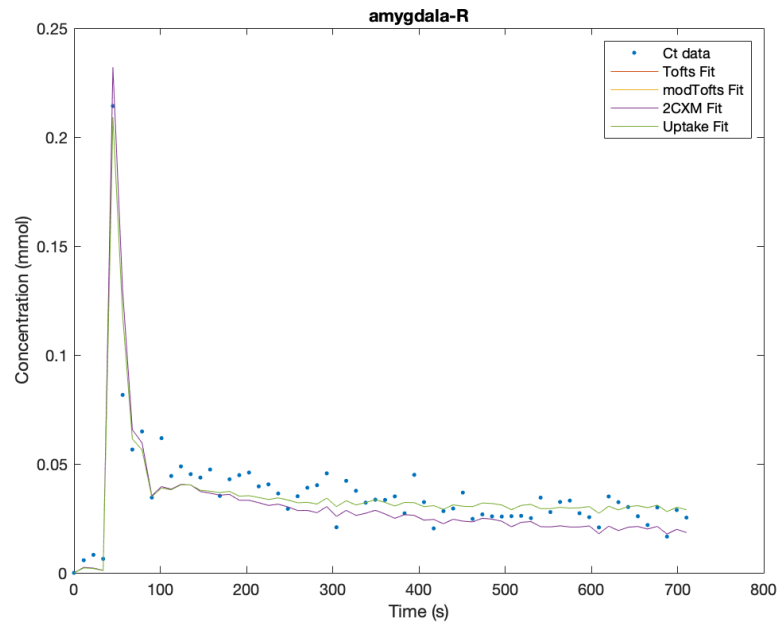


FIGURE 4.2: Concentration-time data within the right amygdala of exam 8126.

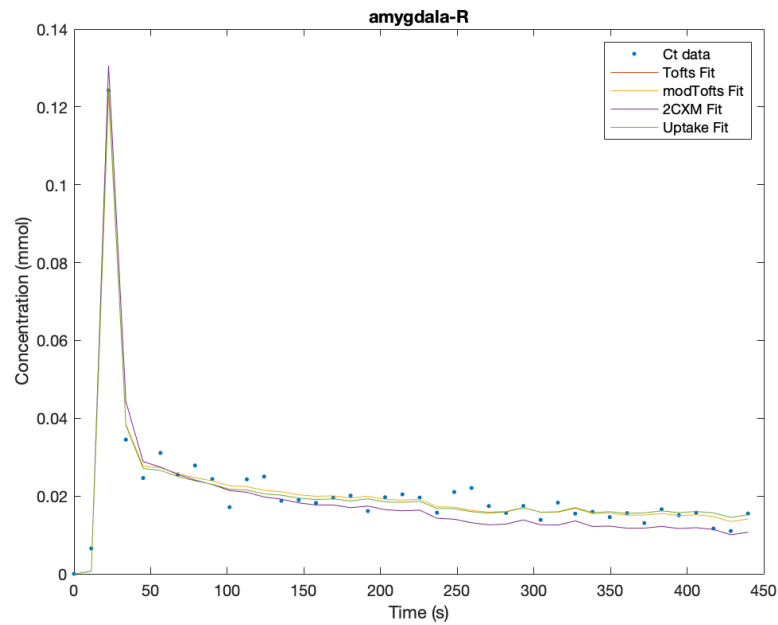


FIGURE 4.3: Concentration-time data within the right amygdala of exam 8239.

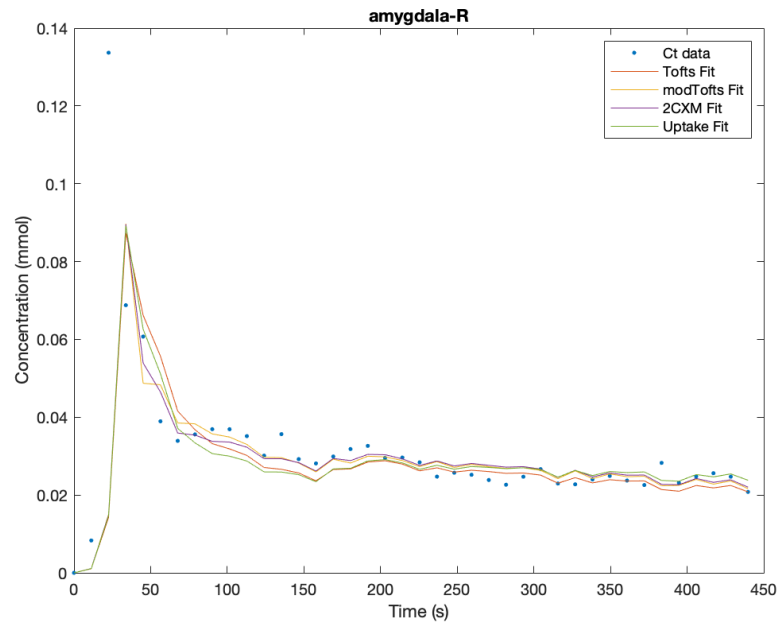


FIGURE 4.4: Concentration-time data within the right amygdala of exam 8264.

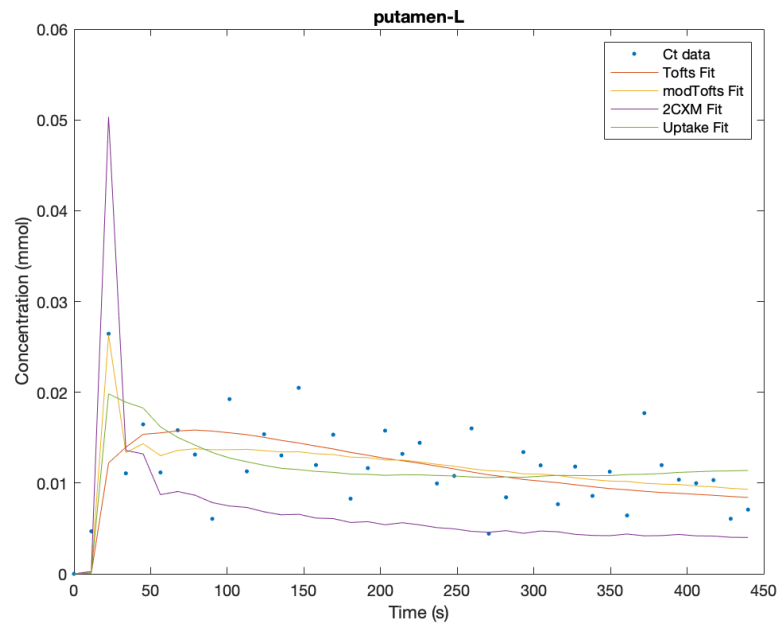


FIGURE 4.5: Concentration-time data within the left putamen of exam 8242.

4.3 Statistical Analysis

An ANOVA test was performed on the models, using data from each scan in each ROI. This test assumed the null-hypothesis that there is no difference between the fits of the models. The p-value of these tests for each ROI were never lower than 0.05, therefore there was no significant difference in performance between the models within the individual ROIs.

TABLE 4.6: Table of ROI and P-values from individual ANOVA tests.

ROI	P-value
Posterior Pituitary	0.3903
Pons	0.2189
Cerebellum	0.1309
Putamen L	0.6006
Putamen R	0.7642
Amygdala L	0.5010
Amygdala R	0.4154
Thalamus L	0.5857
Thalamus R	0.7697
HCN L	0.6384
HCN R	0.7417
Hippocampus L	0.4959
Hippocampus R	0.2246

To investigate other influences on model accuracy, the posterior pituitary accuracy results were analyzed with an ANCOVA model to see the impact of model with a covariant of voxel size. As mentioned in Chapter 3, each subject had a unique ROI drawn for their posterior pituitary since the registration did not accurately map the small region in exactly the same place for each brain. Due to this, there is a variation of posterior pituitary ROI sizes (number of voxels) among the subjects. It is useful to investigate if ROI size has an impact on fit accuracy, since a smaller ROI size would typically mean a lower signal-to-noise ratio, since there are less signals to average.

As seen in figure 4.6, while the dependence on method (called group in the table) is still insignificant, at 0.359, the dependence on ROI size is 0.008, less than the threshold for significance of 0.05, making it a significant contribution to variance. Figure 4.7 shows a graphical representation of the table in figure 4.6, with ROI size along the x-axis, R^2 along the y-axis and the different models colour-coded. From this the difference between models' means and their dependence on ROI size is visualized.

ANOVA Table					
Source	d.f.	Sum Sq	Mean Sq	F	Prob>F
group	3	0.02061	0.00687	1.1	0.359
ROIsize	1	0.04796	0.04796	7.67	0.008
group*ROIsize	3	0.00118	0.00039	0.06	0.9791
Error	48	0.30026	0.00626		

FIGURE 4.6: ANCOVA test results for analysis of model and ROI size contribution to R^2 variance in the posterior pituitary. 'group' refers to model, and ROIsize is number of voxels within the ROI.

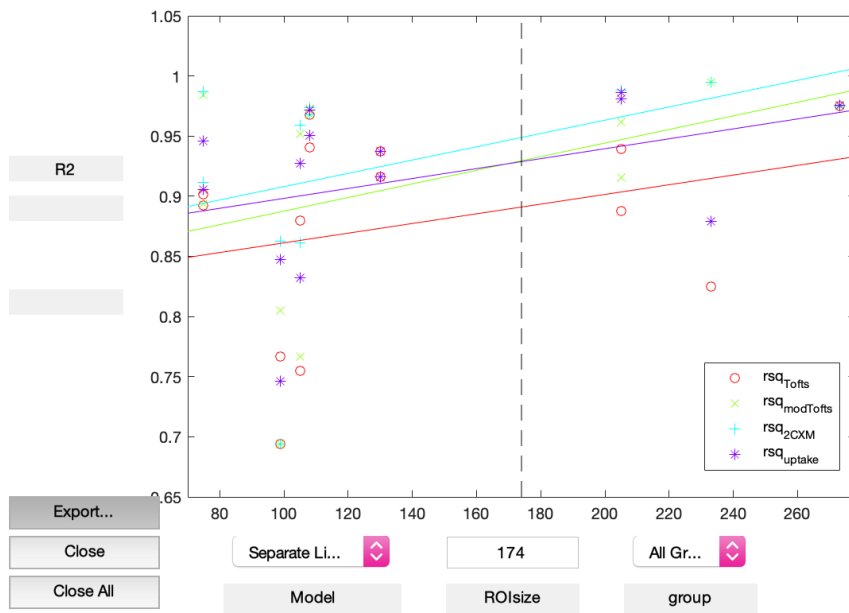


FIGURE 4.7: Graphical representation of ANCOVA test results for posterior pituitary. Different colours correspond to different models, ROIsize (number of voxels within the ROI) is the x-axis), while R^2 is the y-axis.

Individually, the ROIs revealed no significant differences between the accuracy of the four models. However, when all R^2 values in the ROIs with a blood-brain barrier (i.e. all ROIs except the posterior pituitary gland) were tested with an ANOVA test, the Tofts model accuracy had a significantly lower mean than that of the modified Tofts and Uptake models, with a p-value of 0.0068 (figures 4.8 and 4.9).

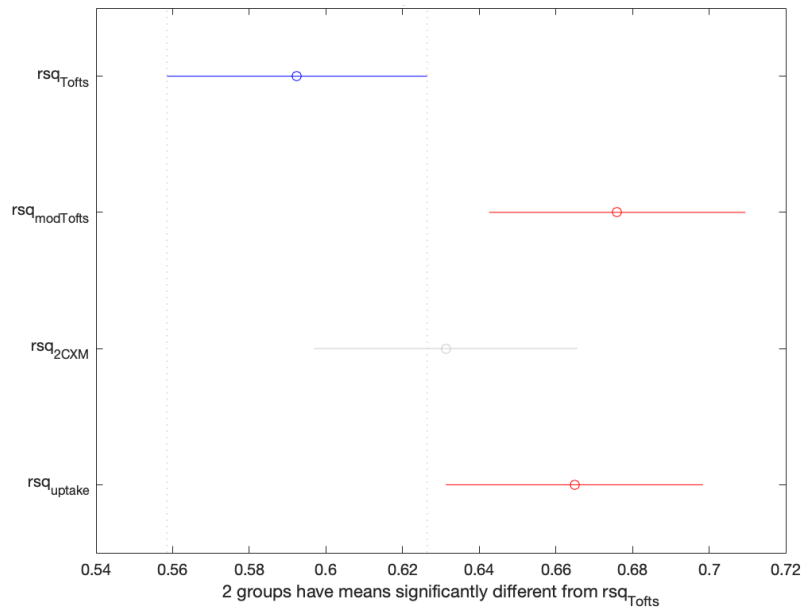


FIGURE 4.8: Matlab plot of R^2 means and comparison intervals according to ANOVA test. A model is significantly different when the comparison interval does not overlap with that of another model.

ANOVA Table					
Source	SS	df	MS	F	Prob>F
Groups	0.7	3	0.23333	4.1	0.0068
Error	37.2021	653	0.05697		
Total	37.9021	656			

FIGURE 4.9: ANOVA test results for all BBB ROIs.

Drawing from the results of the ANCOVA analysis of ROI size covariance done in the posterior pituitary, another ANCOVA test was performed on the BBB ROIs. Again, the Tofts model accuracy was significantly different, with a p-value of 0.006 (figures 4.10 and 4.11). As in the posterior pituitary analysis, this test also showed that ROI size had a significant correlation to R^2 values between ROIs (p-value 0.001). Again, figure 4.11 provides visualization for the differences in R^2 means and their dependence on ROI size.

ANOVA Table					
Source	d.f.	Sum Sq	Mean Sq	F	Prob>F
group	3	0.7075	0.23583	4.19	0.006
ROIsize	1	0.6117	0.61165	10.86	0.001
group*ROIsize	3	0.0305	0.01017	0.18	0.9096
Error	649	36.56	0.05633		

FIGURE 4.10: ANCOVA test results for BBB ROI analysis of model and ROI size contribution to R^2 variance. 'group' refers to model, and ROIsize is number of voxels within the ROI.

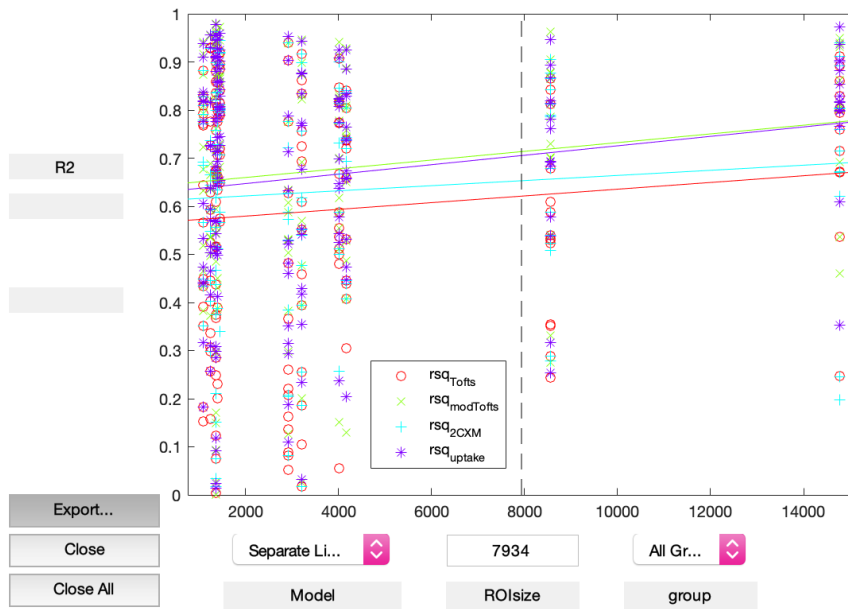


FIGURE 4.11: Graphical representation of ANCOVA test results for BBB ROIs. Different colours correspond to different models, ROIsize (number of voxels within the ROI) is the x-axis, while R^2 is the y-axis.

Chapter 5

Discussion and Conclusions

5.1 Discussion of Results

These results demonstrate the differences between the accuracy of the Tofts model, the modified Tofts model, the Two-Compartment Exchange model, and the Uptake model within areas of the brain with a blood-brain barrier. It was found that the Tofts model had a significantly lower mean R^2 compared to the other three models, with a p-value of 0.0068. Between the remaining models, no significant difference was found, and therefore no conclusions can be drawn about whether there is one which performs better than the others in this particular type of microvasculature. However, since data points were limited to only 14, it is possible that one model does outperform the others, but not significantly enough to tell with the small sample size.

The most significant finding of this project is that the original Tofts model performed significantly worse than the other three models. The main differences between the Tofts model and other models is that it assumes a negligible signal contribution from the v_p , or plasma space. Additionally, along with the modified Tofts model, it assumes that the mean transit time (MTT) is also negligible. However, since the modified Tofts model did not also perform significantly worse, it can be inferred that this assumption is not invalid. With the ROI method that was used in this project, the concentration in the whole ROI was fit with the model, so it is possible that there is a significant amount of plasma space included in the broad ROI. This may have been avoided if a voxel-by-voxel approach had been used, so that voxels with negligible plasma space would have been modelled accurately. However, the Tofts model also would then have encountered issues with voxels that encompass larger (i.e. arteriole/venule) vasculature, leading to inaccuracies there as well. Furthermore, a voxel-wise approach would also suffer from reduced SNR leading to lower fit quality. Nonetheless, in the case of microvasculature possessing a blood-brain barrier, it is more appropriate to use one of the other, higher performing models.

As for the other three models, it was found that there was no significant difference in fit quality. Taking this result at face value, it would be most appropriate to use the model with the least number of parameters, if there is indeed no difference in accuracy. The Uptake and modified Tofts models have three parameters each, making them less computationally heavy than the general 2CXM model. However, for a study with a variety of tissue environments, the 2CXM model may be appropriate due to its generality. For example, if one wanted to study tumours in the brain compared to healthy tissue in the brain, the 2CXM might provide the most accurate results for both of those tissue types. Additionally, the 2010 Donaldson study (Donaldson et al. 2010) saw improved performance in the 2CXM and Uptake models compared to the Tofts models in cervical tumours, supporting its use in higher-permeability tissues.

Comparing the ROIs that possess a BBB to the posterior pituitary (which lacks BBB), the posterior pituitary had the highest R^2 values, and therefore the best fits. This is likely due to the higher amount of tracer in that region, and subsequently higher signal, leading to a higher signal-to-noise ratio. This ties into another aspect which was investigated: the variation of ROI size. In the posterior pituitary the ROI size was notably different for each subject. Including it as a covariate in the ANCOVA analysis (figures 4.6 4.7) accounted for a large contribution to the variance, (ROI size variance had a p-value of 0.008 in the posterior pituitary). ROI size was also used as a covariate when comparing the BBB ROIs, with a significant p-value of 0.001. In both cases, the ROI size was positively correlated with R^2 , meaning a larger ROI (with more voxels) tended to have more accurate fits. This is very likely due to the noise being reduced when more concentration curves were included in the average, again leading to a higher signal-to-noise ratio.

Comparing the calculated PS values for 2CX and Uptake models, as well as comparing the Ktrans values for the Tofts models, shows that these fitted parameters have vastly different values. It was expected that they would be more similar, especially since the R^2 values were not significantly different. But since they were different suggests there is something inaccurate about the fitting that is not described well by the R^2 value. Even in the posterior pituitary, which had R^2 values of at least 0.88, the mean Ktrans values were different by a factor of around 1.5, and the mean PS values differed by a factor of approximately 10. Without a reliable measure of these parameters it is impossible to say which model has achieved the more accurate value.

A weakness in this analysis is that the registration was not always completely accurate, leading to the pre-drawn MNI ROIs not lining up with the actual region in the registered brain. This was most evident with the posterior pituitary MNI ROI, which often completely missed the actual posterior pituitary in subjects, due

to its small size. This region required unique ROIs to be drawn for each subject, as mentioned previously. This was also likely a problem with other ROIs, however in the interest of saving time and streamlining the process unique ROIs were not made for any of the other brain areas. Additionally, some ROIs, like the head of the caudate nucleus and the thalamus, were adjacent to regions of cerebral spinal fluid (CSF). If there was any significant overlap of the ROI into that area it would cause the average concentration curve to be weighted lower, since there should be minimal tracer present in the CSF (over the course of the scanning). In the future, an additional step to mask out voxels with high percentages of CSF, bone, blood, or other distinct matter would help mitigate this problem and have a positive effect on accuracy.

5.2 Significance

A recent study found success using semi-quantitative methods in the brain to detect differences in leakage in control subjects compared to subjects with bipolar disorder (Kamintsky et al. 2020). This method, called the linear method (Chasidim et al. 2013), has the advantage of less strict imaging requirements, for example it does not require the subject to be injected during the scan, and can instead be injected prior to it (although time between injection and scanning should be the same to be able to compare scans). However, as the term suggests, its quantification of leakage is relative to the leakage in a reference ROI, the superior sagittal sinus, and is therefore dimensionless, unlike the quantification with pharmacokinetic modelling, which produces absolute numbers independent of references.

Depending on situation, semi-quantitative methods can offer more flexibility, and relative numbers may be all that is desired. Quantitative measurements of permeability, however, can offer more precise indication of blood-brain barrier disruption, or reveal subtle differences that semi-quantitative cannot. In the aforementioned Kamintsky study, leakage rates were considered pathological when exceeding the 95th percentile of a control group (Weissberg et al. 2014). Subjects with abnormally high overall BBB leakage were found using outlier analysis, defined as two standard deviations from the median leakage, based on all 50 subjects involved (36 bipolar subjects, 14 control subjects, matched for age, sex and metabolic status). All ten subjects, who demonstrated extensive leakage, were in the bipolar group. These patients were also found to have more severe depression and anxiety. In a similar study, quantification may be useful in revealing the more subtly enhanced leakage in the remaining 26 bipolar subjects, if it exists. One final note: the study found that BBB disruption tended to be "diffuse rather than focal," which leaves the question: was the reference ROI also impacted by higher

leakage? In which case the semi-quantitative leakage rates would be a biased form of measurement.

As mentioned, this study drew inspiration from a 2010 study by Donaldson et al. That study compared the same four methods in a very different tissue environment- that of cervical carcinoma. Tumour microvasculature is known for being highly permeable, as to maximize nutrient delivery to the tumour, which is in stark contrast to the strict blood-brain barrier. The Donaldson study hypothesized that both the original and modified Tofts would be inferior models to the Two-Compartment Exchange and Uptake models due to their assumption of negligible plasma mean transit time (MTT). Their hypothesis was supported by the findings of the study, which did indicate that the 2CX and Uptake models performed better. They also found a mean plasma MTT of 22 ± 16 s, which is a significant amount of time. In the brain, however, the modified Tofts model did not perform significantly different than those models, even having the highest R^2 mean of all the models, which suggests that the assumption of negligible MTT is appropriate under these conditions. This is further supported by the mean MTT values found in this study, which were less than 0.5 s in all ROIs (table 4.5).

In 2020, a study was published by Ohene et al. investigating BBB permeability in mice using one of the alternative techniques mentioned in Chapter 1, arterial spin labelling (ASL) MRI (Ohene et al. 2021). As mentioned, this technique has the benefit of not requiring intravenous contrast agent, as it measures the perfusion of endogenous water in the blood through the BBB. Additionally, in a 2018 study comparing ASL to DCE-MRI, ASL detected increased water perfusion in a rat model of Alzheimer's disease (AD) while DCE-MRI failed to detect any increased permeability within afflicted rats (Dickie et al. 2019). Additionally, the ASL in the Dickie study did enable quantification of the water perfusion. Even more recently, ASL was used to detect BBB breakdown in humans, and compared it with a contrast-based MRI technique- however, not DCE-MRI (Lin et al. 2021). The increased sensitivity to BBB disruption by the ASL method could very well be due to the fact that water is much smaller (18 Daltons) than Gd chelates (500-600 Daltons). From these results, ASL seems to be a promising modality for detecting the subtle BBB dysfunction this project is concerned with.

5.3 Future Directions

These results show a clear difference between the accuracy of certain pharmacokinetic models, which can aid in the decision of which model is most appropriate in a given situation. Unfortunately, given the limited amount of data sets, the differences between the three top-performing models remain inconclusive. There

are still more areas of interest to be investigated within the scope of this project, as well as outside of it.

With the available data, several venues could be further assessed to potentially improve results. The aforementioned tissue segmentation to exclude non-brain-matter from the ROIs would be possible to implement. Additionally, rather than using ROI size as an indicator of SNR, the actual SNR in an ROI could be calculated and used as a covariate in the statistical analysis. This would help to tease out the contribution of noise to any inaccuracy of fit for the comparison of all BBB ROIs, and leave behind the dependence on model. Both of these improvements would give a better representation of the accuracy of each model, and could possibly reveal differences in the remaining three models that were previously hidden by those other contributions to variance. If more data were to be acquired, it might also reveal these differences. Finally, a whole-brain analysis could be done voxel-by-voxel to provide images that map the permeability over the entire brain, rather than solely the ROIs that were chosen.

Beyond this project, the findings could be useful in other clinical studies looking at disruptions in the BBB, specifically those looking for subtle disruption and quantitative results. It would be interesting to test the two orders of concentration calculation discussed in Chapter 3, in the section titled "Order of Concentration Calculation" in more types of tissue to validate that this order does matter (or prove that it doesn't). It will also be exciting to see if ASL proves to be a better modality for subtle detection of BBB breakdown, and to see a comparison between it and DCE-MRI.

Appendix A

Code

A1 Pre-Processing

A1.1 Registration with FSL

T1-map-prep-batch-2020

Unix executable

Used to convert dicom files to NIFTI and register images in preparation for T1 map generation and DCE analysis

Created by Norm Konyer, modified by Ashley Gilbank

```
#!/bin/csh
clear
echo "#####"
echo "Program to prep data for T1 map program."
echo "Initially for B. Frey BBB project. T1 analysis by Kim Desmond"
echo " "
echo "Norm Konyer"
echo "Created: 28 Jun 2018"
echo "Modified: July 6th, 2019 by M. Noseworthy"
echo "Modified: July 22nd, 2019 by A. Gilbank"
echo "Modified: November 16th, 2020 by A. Gilbank"
echo "Questions? Still go ask.... nkonyer@stjoes.ca"
echo " "
echo "#####"
echo "-----"
echo "Convert dicom images to nifti"
echo "Put this script somewhere in your path, preferably ~/bin"
echo "Note: you should be in DATA/BBB_exams directory"
echo "-----"
echo " "
```

```
pwd
```

```
foreach i ( exam_* )
```

```
#set exam1='echo $i | rev | cut -c -4'  
#set exam='echo $exam1 | rev'
```

```
set exam = 'echo $i'
```

```
#echo "----- exam_$exam -----"  
echo "----- $exam -----"
```

```
echo " "  
#ls -ltr exam_{$exam}  
ls -ltr {$exam}  
echo " "
```

```
#cd exam_{$exam}  
cd {$exam}
```

```
# more seriesINFO*
```

```
echo " "  
echo " "
```

```
# series number for 3DT1 (Ax FSPGR 3D) pre-Gd scan:
```

```
set T13D = "3"
```

```
# series number for 3DT1 (Ax FSPGR 3D POST GAD C+) post-Gd scan:
```

```
set T13Dgd = "11"
```

```
echo " "
```

```
# 3 imaging sequences for T1 mapping
```

```
# series number for 3D T1W BRAVO scan:
```

```
set T1W = "7"
```

```
# series number for 3D PDW FLASH scan:
```

```
set PDW = "8"
```

```
# series number for B1 map scan:
```

```
set B1map = "9"
```

```
# Time series data
```

```
# series number for resting state scan:
```

```
set rest = "5"
```

```
# series number for dceMRI scan:
```

```
set DCE = "10"
```

```
# series number for B0 map scan:
```

```
set B0map = "6"
echo " "
echo " "
echo -n "ALIGNMENT to MNI152 (m) or to initial 3DT1 (i) ?: "
set align = "m"

# Make Nifti (nii) files
# these can all be viewed with FSL, AFNI or Matlab (need Nifit toolbox)

# pre and post 3D contrast T1
/usr/local/bin/dcm2niix -o ./ -f %s Ser{${T13D}}
mv {${T13D}}.nii T13dpre.nii
/usr/local/bin/dcm2niix -o ./ -f %s Ser{${T13DGd}}
mv {${T13DGd}}.nii T13dpost.nii

# Data for T1 mapping
/usr/local/bin/dcm2niix -o ./ -f %s Ser{${T1W}}
mv {${T1W}}.nii T1W.nii
/usr/local/bin/dcm2niix -o ./ -f %s Ser{${PDW}}
mv {${PDW}}.nii PDW.nii
/usr/local/bin/dcm2niix -o ./ -f %s Ser{${B1map}}
mv {${B1map}}.nii B1map.nii

# Time series data
/usr/local/bin/dcm2niix -o ./ -f %s Ser{${rest}}
mv {${rest}}.nii rest.nii
/usr/local/bin/dcm2niix -o ./ -f %s Ser{${DCE}}
mv {${DCE}}.nii DCE.nii
/usr/local/bin/dcm2niix -o ./ -f %s Ser{${B0map}}
mv {${B0map}}.nii B0map.nii

# get rid of these json files- no idea what they're for anyway!
rm *.json

# make a directory for original DICOMs and move them there to be safe
# mkdir originalDATA
# cp Ser* originalDATA

echo " "
echo " Run alignment now "
echo " "
```

```
# -----  
  
if ($align == "m") then  
  
mkdir regMNI  
cd regMNI  
  
else  
  
mkdir regSELF  
cd regSELF  
  
endif  
  
# register PD and B1map to original T1, put results in regMRI  
  
flirt -in ../PDW.nii -ref ../T1W.nii -out PDW_reg_T1W.nii -omat  
    PDW_reg_T1W.mat -dof 12 -interp trilinear -v  
  
flirt -in ../B1map.nii -ref ../T1W.nii -out B1map_reg_T1W.nii -omat  
    B1map_reg_T1W.mat -dof 12 -interp trilinear -v  
  
flirt -in ../DCE.nii -ref ../T1W.nii -out DCE_reg_T1W.nii -omat  
    DCE_reg_T1W.mat -dof 12 -interp trilinear -v  
  
if ($align == "m") then  
  
# register T1 to MNI152, put result in regMNI  
  
# make sure the file MNI152_T1_1mm.nii is in the path, or modify this  
    file to point directly to it  
  
flirt -in ../T1W.nii -ref ~/MNI152_T1_1mm.nii -out T1W.nii -omat T1W.mat  
    -dof 12 -interp trilinear -v  
  
# -----  
  
# determine transformation matrices
```

```
convert_xfm -omat PDW_T1W_MNI.mat -concat T1W.mat PDW_reg_T1W.mat

convert_xfm -omat B1map_T1W_MNI.mat -concat T1W.mat B1map_reg_T1W.mat

convert_xfm -omat DCE_T1W_MNI.mat -concat T1W.mat DCE_reg_T1W.mat

# apply tranformations on PD and B1maps
flirt -in ../PDW.nii -applyxfm -init PDW_T1W_MNI.mat -out PDW.nii -ref
      T1W.nii -paddingsize 0.0 -interp trilinear -v

echo " PDW transformed. "

flirt -in ../B1map.nii -applyxfm -init B1map_T1W_MNI.mat -out B1map.nii
      -ref T1W.nii -paddingsize 0.0 -interp trilinear -v

echo " B1map transformed. "

flirt -in ../DCE.nii -applyxfm -init DCE_T1W_MNI.mat -out DCE.nii -ref
      T1W.nii -paddingsize 0.0 -interp trilinear -v

echo " DCE transformed. "

# remove intermediate data

#rm B1map_reg_T1W.nii.gz B1map_reg_T1W.mat PDW_reg_T1W.nii.gz
      PDW_reg_T1W.mat DCE_reg_T1W.nii.gz DCE_reg_T1W.mat

endif

gunzip *.gz
# new aligned files are B1map.nii PDW.nii and T1W.nii in directory
      regMNI or regSELF
cd ..

#
-----

# registering to high res anatomical scan. Don't want to do that rn.
if ( 0 ) then
```

```
mkdir regSELF

# register to pre contrast 3D T1, put result in regSELF
# make sure the file MNI152_T1_1mm.nii is in the path, or modify this
  file to point directly to it

flirt -in T1W.nii -ref T13dpre.nii -out regSELF/T1W.nii -omat regSELF/
  T1W.mat -dof 12 -interp trilinear -v

# register PD and B1map to original T1, put results in regSELF

flirt -in PDW.nii -ref T1W.nii -out regSELF/PDW_reg_T1W.nii -omat
  regSELF/PDW_reg_T1W.mat -dof 12 -interp trilinear -v
flirt -in B1map.nii -ref T1W.nii -out regSELF/B1map_reg_T1W.nii -omat
  regSELF/B1map_reg_T1W.mat -dof 12 -interp trilinear -v

# determine transformation matrices

convert_xfm -omat regSELF/PDW_T1W_MNI.mat -concat regSELF/T1W.mat
  regSELF/PDW_reg_T1W.mat
convert_xfm -omat regSELF/B1map_T1W_MNI.mat -concat regSELF/T1W.mat
  regSELF/B1map_reg_T1W.mat

# apply transformations on PD and B1maps

flirt -in PDW.nii -applyxfm -init regSELF/PDW_T1W_MNI.mat -out regSELF/
  PDW.nii -ref regSELF/T1W.nii -padding 0.0 -interp trilinear -v
flirt -in B1map.nii -applyxfm -init regSELF/B1map_T1W_MNI.mat -out
  regSELF/B1map.nii -ref regSELF/T1W.nii -padding 0.0 -interp
  trilinear -v

# remove intermediate data
cd regSELF
rm B1map_reg_T1W.nii.gz B1map_reg_T1W.mat PDW_reg_T1W.nii.gz PDW_reg_T1W
  .mat
# didn't work (rm: B1map_reg_T1w.nii.gz) -- because it's .nii and not .
  nii.gz? can easily check... l8r
```



```
gunzip *.gz
# new aligned files are B1map.nii PDW.nii and T1W.nii in directory
    regSELF
cd ..

endif

#
-----

cd ..

end

echo "-----"
echo "-fin-"
exit
```

A1.2 Generating T1 Map

pipeline.m

Matlab function

Created by Norm Konyer, modified by Ashley Gilbank

```
function T1_im = pipeline(experiment,reg_reference)
tic

addpath('/Users/ashleygilbank/Documents/DATA')
addpath('/Users/ashleygilbank/Documents/DATA/T1map')
addpath('/Users/ashleygilbank/Documents/DATA/NIfTI_20140122') % this is
    the file with functions for reading nii files etc.
addpath('/Users/ashleygilbank/Documents/DATA/nearestpoint')

root = [pwd filesep];
%
% this gives something like: root = /user/norm/example_data
% filesep in this case = /
%
%exam = 6391;
```

```
%exam = input('Enter exam number: ');
%experiment = ['exam_' num2str(exam) filesep];
exam = experiment(6:9); % getting just the number
experiment = [experiment filesep];
fpath = [root experiment];

%reg_reference = input('Enter registration reference (1 for MNI152 or 2
    for initial 3DT1): ');
if reg_reference == 1
    direc = 'regMNI/';
else
    direc = 'regSELF/';
end

fid = fopen([root experiment 'seriesINFO-' num2str(exam)]);

tline = fgetl(fid); %discard first line
while ~feof(fid)
    tline = fgetl(fid);
    series = sscanf(tline(9:30), '%d');
    if ~isempty(strfind(tline,'SAG BRAVO WHOLE BRAIN'))
        T1W_series = series;
    end

    if ~isempty(strfind(tline,'*SAG FLASH PD'))
        PDW_series = series;
    end

    if ~isempty(strfind(tline, 'B1 map'))
        B1_series = series;
    end
end

end
% B1 map not used at this point.
B1 = load_nii([fpath direc 'B1map.nii']); % regMNI because that's where
    the registered files will be now...
PDW = load_nii([fpath direc 'PDW.nii']); % no .gz because Dr. N's T1-
    prep2 code unzips them
T1W = load_nii([fpath direc 'T1W.nii']);
%B1_corr = ones(size(PDW(:,:,,1)));
B1_corr = double(B1.img)./150; %divide by 10*nominal flip.

IE = 1;
toc
```

```
tic
summedRepetitions = 1;
cvFactorT1W = summedRepetitions*computeCVscaleFactor([root experiment '
    Ser' num2str(T1W_series) filesep 'E' num2str(exam) 'S' num2str(
    T1W_series) 'I001.MR']);
cvFactorPDW = summedRepetitions*computeCVscaleFactor([root experiment '
    Ser' num2str(PDW_series) filesep 'E' num2str(exam) 'S' num2str(
    PDW_series) 'I001.MR']);
toc
disp('computeCVscaleFactor done')
tic
%generate the images in units of T1 (ms):

if exist('lookupTable.mat')
    load('lookupTable.mat');
else
    lookupTable = MPRAGE_lookup_table_generate('
        SAG_BRAVO_WHOLE_BRAIN_BOCK_FREY_ICM_CIHR', '
        SAG_FLASH_PD_BOCK_FREY_ICM_CIHR', IE); %this only has to be
        generated once if IE stays the same.
    save('lookupTable', 'lookupTable');
end
toc
disp('look up table loaded')
tic
T1_im = MPRAGE_lookup(double(T1W.img)./cvFactorT1W, double(PDW.img)./
    cvFactorPDW, B1_corr(:,:,1), lookupTable); %with B1 correction
%T1_im = MPRAGE_lookup(double(T1W.img)/cvFactorT1W, double(PDW.img)/
    cvFactorPDW, ones(size(B1_corr(:,:,1))), lookupTable); %no B1
    correction.
%display the middle slice
toc
tic

figure;imagesc(T1_im(:,:,91));colorbar;

toc
% save the resulting T1 image as matlab file in exam root directory:
outt1 = [fpath direc 'T1_im.mat'];
save(outt1, 'T1_im');

function cvFactor = computeCVscaleFactor(fname)
```

```
%get sequence parameters from the dicom header
%dicom intensity does NOT change with RG or ARC
%depends on the number of voxels.

tmp = dicominfo(fname); %grab the dicom header of the first image.
%RG = tmp.Private_0019_1095; %analog receive gain (doesn't impact signal
    amplitude, KLD 20180404)
RG = 1;
read = double(tmp.Height);
readforBW = double(tmp.Rows);
pe1 = double(tmp.Private_0021_1057); %within "tau" for MPRAGE
pe2 = double(tmp.Width);
Nvoxels = read*pe1*pe2;
bandwidth = tmp.PixelBandwidth*readforBW;
cvFactor = double(RG)*sqrt(Nvoxels)/sqrt(bandwidth);

pipeline_batch.m
Apply pipeline.m to all exams in a folder

experiment = dir('exam_*');

reg_reference = 1; % 1 for regMNI, 2 for regSELF

for i = 1:length(experiment)
    disp(experiment(i).name);
    disp(' ');
    pipeline(experiment(i).name,reg_reference);
end

disp(' ---- END ---- ')
```

A2 Processing

A2.1 Main Function

BBB_2020.m

Fits data with all four methods (main)

```
function BBB_2020(exam)

addpath('/Users/ashleygilbank/Documents/DATA/NIfTI_20140122') % this is
    the file with functions for reading nii files etc.
% root = [pwd filesep 'BBB_exams/'];
root = [pwd filesep 'BBB_exams/'];
% pwd is DATA folder
% root = ['/Users/ashleygilbank/Documents/DATA' filesep]; % since I
    should be there every time? will this work?
%
% this gives something like: root = /user/norm/example_data
% filesep in this case = /
%

% ex exam = 8126
experiment = ['exam_' num2str(exam) filesep];
% ex experiment = 'exam_8126/'
fpath = [root experiment];

reg_reference = 1;

if reg_reference == 1
    direc = 'regMNI/';
else
    direc = 'regSELF/';
end

folder1 = [fpath direc];

% ----- load T1_map and masks -----

% load T1 map
load([folder1 'T1_im.mat'], 'T1_im');
```

```
% loading DCE
% don't reload unless you have to!
if not(exist('DCE_nii')) || (exist('DCE_nii') && all(DCE_nii~= [folder1 '
    DCE.nii'] )
    DCE_nii = [folder1 'DCE.nii'];
    DCE = load_nii(DCE_nii);
end

DCE_img = double(DCE.img);

% finding AIF from MCA ROI (and average T10)

[AIF] = findAIF(DCE_img,T1_img);

% T1_voxels = T1_img(:);

process_ROI('amygdala-L',fpath,T1_img,DCE_img,AIF,folder1,root)
process_ROI('amygdala-R',fpath,T1_img,DCE_img,AIF,folder1,root)
process_ROI('putamen-L',fpath,T1_img,DCE_img,AIF,folder1,root)
process_ROI('putamen-R',fpath,T1_img,DCE_img,AIF,folder1,root)
process_ROI('cerebellum',fpath,T1_img,DCE_img,AIF,folder1,root)

process_ROI('hippocampus-L',fpath,T1_img,DCE_img,AIF,folder1,root)
process_ROI('hippocampus-R',fpath,T1_img,DCE_img,AIF,folder1,root)
process_ROI('HofCN-L',fpath,T1_img,DCE_img,AIF,folder1,root)
process_ROI('HofCN-R',fpath,T1_img,DCE_img,AIF,folder1,root)
process_ROI('thalamus-L',fpath,T1_img,DCE_img,AIF,folder1,root)
process_ROI('thalamus-R',fpath,T1_img,DCE_img,AIF,folder1,root)

process_ROI('post_pituitary',fpath,T1_img,DCE_img,AIF,folder1,root)
process_ROI('pons',fpath,T1_img,DCE_img,AIF,folder1,root)

% for reference:
% load('test.mat')

disp('done!');
```

end

A2.2 Sub-Functions

Finding Concentration from Signal

```
function C_t = getConcentration(sig,T10)

% from Rohrer 2005
R1 = 5.0; % L/smM at 3T
R2 = 7.1; % L/smM at 3T

TRms = 3.8; % ms
TEms = 1.2;
TE = TEms/1000;
TR = TRms/1000;

% converting signal to concentration
NS = sig/sig(1);

theta = 30*pi/180; % value we use

C = sin(theta)*(1-exp(-TR/T10))/(1-cos(theta)*exp(-TR/T10));
% eqn1 = E == (exp(-TE*R2*Ct)*sin(theta)*((1-exp(-TR*((1/T_10)+R1*Ct)))
    /(1-cos(theta)*exp(-TR*((1/T_10)+R1*Ct))))-C)/C;

% find peak signal for this voxel's T10
t_peak=linspace(0,100,10000); % x1(t1)-- t1 is a concentration
x_peak=(exp(-TE.*R2.*t_peak).*sin(theta).*(1-exp(-TR.*((1/T10)+R1.*
    t_peak))))./(1-cos(theta).*exp(-TR.*((1/T10)+R1.*t_peak))))/C;
[M,I] = max(x_peak);
if max(NS)>M
    disp(['Maximum signal is higher than theoretical: ' num2str(max(NS))
        ' > ' num2str(M)]);
end
peak = t_peak(I);

% NEW, FAST, LESS PRECISE WAY:
t1=linspace(0,peak,1000); % x1(t1)-- t1 is a concentration
```

```
x1=(exp(-TE.*R2.*t1).*sin(theta).*(1-exp(-TR.*((1/T10)+R1.*t1)))/(1-cos(theta).*exp(-TR.*((1/T10)+R1.*t1))))/C;
C_t=NS*0;

% SO MUCH FASTER:
for x = 1:length(NS)
    diff=abs(x1-NS(x));
    [~,I]=min(diff);
    C_t(x)=t1(I);
end

% OLD, SLOW, VPASOLVE WAY:
% syms Ct
% eqn1 = (exp(-TE.*R2.*Ct).*sin(theta).*(1-exp(-TR.*((1/T_10)+R1.*Ct)))/(1-cos(theta).*exp(-TR.*((1/T_10)+R1.*Ct))))/C;
%
%
% for x = 1:length(NS)
%     if NS<21.7
%         NS_eqn = NS(x);
%         C_t(x)=vpasolve(eqn1==NS_eqn);
%     else
%         Ct=31.11; % band-aid fix... because the max of eqn is 21.7 at
%         Ct = 31.111, so idk what to do
%     end
% end
end
```

Processing Each ROI

```
function process_ROI(ROI,fpath,T1_im,DCE_img,AIF,folder1,root)

% ROI = 'hippocampus','post_pituitary','HofCN','thalamus','pons'

% ----- load masks -----

% load masks
mask_file = ['~/Documents/DATA/MNI_masks/MNI152_T1_1mm-' ROI '-mask.nii.gz'];

if strcmp(ROI,'post_pituitary')
    mask_file = [fpath 'regMNI/T1W_mask_post_pituitary.nii.gz'];
end
```



```
mask = load_nii(mask_file);

mask_img = double(mask.img);

scan_time = (7*60 + 31)/40; % length of each scan
size_DCE = size(DCE_img);
time_points=size_DCE(4);
total_scan_time = scan_time*time_points; % 7min 31sec in seconds

scan_length = total_scan_time/time_points; % length of each scan (delta
t)
t= 0:scan_length:(total_scan_time-1);

% masking DCE and T1map
DCE_ROI = DCE_img.*repmat(mask_img,[1 1 1 time_points]);

% reshaping
% make 2D matrix of all voxels' time signals (not volume anymore, list
ofvoxels)
DCE_signals=reshape(DCE_ROI,[size_DCE(1)*size_DCE(2)*size_DCE(3),
size_DCE(4)]); % reshape to be a 2D matrix where each row is an AIF
signal

T1_voxels = T1_im(:);

% isolate nz voxels
ind = find(DCE_signals(:,1));
nzDCE_sigs=DCE_signals(ind,:);
nzT1 = T1_voxels(ind);

% find concentration curves for signals
DCE_Ct_curves = zeros(size(nzDCE_sigs));

for i=1:length(ind)
    DCE_Ct_curves(i,:) = getConcentration(nzDCE_sigs(i,:),nzT1(i));
end

DCE_Ct = transpose(squeeze(mean(DCE_Ct_curves,1)));
```

```
% -----
[Ktrans_T,ve_T,rsq_Tofts,Ct_fit_Tofts] = fit_Tofts(DCE_Ct,AIF,t);
[vp_mT,Ktrans_mT,ve_mT,rsq_modTofts,Ct_fit_modTofts] = fit_modTofts(
    DCE_Ct,AIF,t);
[vp_2,PS_2,ve_2,Fp_2,k01_2,k12_2,k21_2,rsq_2CXM,Ct_fit_2CXM] = fit_2CXM(
    DCE_Ct,AIF,t);
[vp_u,PS_u,Fp_u,y_u,rsq_uptake,Ct_fit_uptake] = fit_uptake(DCE_Ct,AIF,t)
;
% -----

% plotting
figure;plot(t,DCE_Ct, '.',t,Ct_fit_Tofts,t,Ct_fit_modTofts,t,Ct_fit_2CXM,
    t,Ct_fit_uptake);
title(ROI);legend('Ct data','Tofts Fit','modTofts Fit','2CXM Fit','
    Uptake Fit');xlabel('Time (s)');ylabel('Concentration');

% saving

%{%
cd(folder1);
save([ROI '-results.mat'],'rsq_Tofts','rsq_modTofts','rsq_2CXM','
    rsq_uptake','Ktrans_T','ve_T','vp_mT','Ktrans_mT','ve_mT','vp_2','
    PS_2','ve_2','Fp_2','k01_2','k12_2','k21_2','vp_u','PS_u','Fp_u','y_u
');
cd(root);
cd ..
%}

% for reference:
% load('test.mat')

end
```

Finding Arterial Input Function

```
function [AIF_Ct] = findAIF(DCE_img,T1map) % inputs must be double

mask_file = '~/Documents/DATA/MNI_masks/DCE-mask-MCA.nii.gz';
AIF_mask = load_nii(mask_file);
AIF_mask_img = double(AIF_mask.img);
```

```
size_DCE = size(DCE_img);

%T1mapROI=T1map.*AIF_mask_img;

DCE_ROI = DCE_img.*repmat(AIF_mask_img,[1 1 1 size_DCE(4)]);

% make 2D matrix of all voxels' time signals (not volume anymore, list
of voxels)
AIF_signals=reshape(DCE_ROI,[size_DCE(1)*size_DCE(2)*size_DCE(3),
size_DCE(4)]); % reshape to be a 2D matrix where each row is an AIF
signal
%T1_voxels=reshape(T1map,[size_DCE(1)*size_DCE(2)*size_DCE(3),1]);
T1_voxels = T1map(:);

% isolate nz AIF voxels
ind = find(AIF_signals(:,1));
nzAIF_sigs=AIF_signals(ind,:);
nzT1_voxels = T1_voxels(ind);

max_AIF = max(nzAIF_sigs(:,1:floor(size_DCE(4)/2)), [],2); % finding peak
of signal in each voxel (IN FIRST HALF OF SIGNAL)
%max_AIF = max(nzAIF_sigs, [],2);
%mean_AIF = mean(nzAIF_sigs(:)); % finding mean of overall signal
%mean_max = mean(max_AIF);
enhancement = max_AIF./nzAIF_sigs(:,1);
mean_enh = mean(enhancement);
AIF_ind = find(enhancement>mean_enh*5); % finding peak signals that are
above five times the mean of the max...

AIF_maxsignals = nzAIF_sigs(AIF_ind,:); % isolating chosen signals
T10_maxsignals = nzT1_voxels(AIF_ind);

scan_time = (7*60 + 31)/40; % length of each scan
size_DCE = size(DCE_img);
time_points=size_DCE(4);
total_scan_time = scan_time*time_points;
scan_length = total_scan_time/time_points; % length of each scan (delta
t)
t = 0:scan_length:(total_scan_time-1);

% find concentration curves for signals
```

```
AIF_Ct_curves = zeros(size(AIF_maxsignals));

for i=1:length(AIF_ind)
    AIF_Ct_curves(i,:) = getConcentration(AIF_maxsignals(i,:),
        T10_maxsignals(i));
end

AIF_Ct = transpose(squeeze(mean(AIF_Ct_curves,1)));

figure;plot(t,AIF_Ct);title('AIF');xlabel('Time point');ylabel('
    Concentration');

end
```

Finding R^2

```
function rsq = find_rsq(y,yfit)
yresid = y-yfit;
SSresid = sum(yresid.^2);
SStotal = (length(y)-1)*var(y);
rsq = 1-SSresid/SStotal;
end
```

A2.3 The Four Models

Tofts Model

```
function [Ktrans,ve,rsq,Ct_fit] = fit_Tofts(Ct,Cp,t)

% RTofts = Ktrans*exp(-Ktrans*t/ve);
% Ct_model = conv(Cp,RTofts);

dt = diff([t(1),t(2)]);

inputs = [Cp(:),t(:)];

Ct_model = @Tofts_fun;

beta0 = [0;0.5];
%figure;plot(t,Ct_model(beta0,t));
%beta = nlinfit(inputs,Ct,Ct_model,beta0); % Feb 24th test
[beta,resnorm] = lsqcurvefit(Ct_model,beta0,inputs,Ct,[0;0;0],[1;1;1]);
```

```
Ktrans = beta(1);
ve = beta(2);
disp(['Ktrans = ' num2str(Ktrans)]);
disp(['ve = ' num2str(ve)]);

% display fit

Ct_fit = conv(Cp,Ktrans*exp(-Ktrans*t/ve))*dt;
Ct_fit = transpose(Ct_fit(1:length(t)));

%figure;plot(t,Ct, '.',t,Ct_fit);title('Tofts Model');legend('Ct data','
    Ct fit');xlabel('Time (s)');ylabel('Concentration');

%{
Ktrans_test = 0.01;
ve_test = 0.05;

Ct_test = conv(Cp,Ktrans_test*exp(-Ktrans_test*t/ve_test))*dt;
figure;plot(t,Ct, '.',t,Ct_test(1:length(t)));title('Tofts Model test');
    legend('Ct data','Ct test');xlabel('Time (s)');ylabel('Concentration
    ');
%}
rsq = find_rsq(Ct,Ct_fit);
disp('done')
end

function Ct_model = Tofts_fun(b,inputs)

dt = diff([inputs(1,2),inputs(2,2)]);

% Ct_model = @(b,t) conv(Cp,Ktrans*exp(-Ktrans*t/ve));
% Ct_model = @(b,t) conv(Cp,b(1)*exp(-b(1)*t/b(2)))*dt;

Ct_model = conv(inputs(:,1),b(1)*exp(-b(1)*inputs(:,2)/b(2)))*dt;

Ct_model = Ct_model(1:length(inputs(:,2)));

end
```

Modified Tofts Model

```
function [vp,Ktrans,ve,rsq,Ct_fit] = fit_modTofts(Ct,Cp,t)
```

```
% RTofts = Ktrans*exp(-Ktrans*t/ve);
% Ct_fit = vp*Cp + conv(Cp,RTofts);

% Dec 4: not complete

% RTofts = Ktrans*exp(-Ktrans*t/ve);
% Ct_model = conv(Cp,RTofts);

dt = diff([t(1),t(2)]);

inputs = [Cp(:),t(:)];

Ct_model = @modTofts_fun;

beta0 = [0.1;0.5;0.5];
%figure;plot(t,Ct_model(beta0,t));
%beta = nlinfit(inputs,Ct,Ct_model,beta0); % doesn't fit, inf or NaN
      values
%for some reason, I don't know
[beta,resnorm] = lsqcurvefit(Ct_model,beta0,inputs,Ct,[0;0;0],[1;1;1]);

Ktrans = beta(1);
ve = beta(2);
vp = beta(3);
disp(['Ktrans = ' num2str(Ktrans)]);
disp(['ve = ' num2str(ve)]);
disp(['vp = ' num2str(vp)]);

% display fit

Ct_fit_conv = conv(inputs(:,1),Ktrans*exp(-Ktrans*inputs(:,2)/ve))*dt;
Ct_fit = vp*inputs(:,1) + Ct_fit_conv(1:length(inputs(:,2)));
%figure;plot(t,Ct, '.',t,Ct_fit(1:length(t)));title('Modified Tofts Model
');legend('Ct data','Ct fit');xlabel('Time (s)');ylabel('
Concentration');

%figure;plot(t,Ct, '.',t,modTofts_fun(beta,inputs));title('Modified Tofts
Model');legend('Ct data','Ct fit');xlabel('Time (s)');ylabel('
Concentration');

%{
```

```
Ktrans_test = 0.01;
ve_test = 0.05;
vp_test = 0;

Ct_test_conv = conv(inputs(:,1),Ktrans_test*exp(-Ktrans_test*inputs(:,2)
    /ve_test))*dt;
Ct_test = vp_test*inputs(:,1) + Ct_test_conv(1:length(inputs(:,2)));
figure;plot(t,Ct, '.',t,Ct_test(1:length(t)));title('Modified Tofts Model
    test');legend('Ct data','Ct test');xlabel('Time (s)');ylabel('
    Concentration');

disp(['resnorm = ',num2str(resnorm)]);
%}

rsq = find_rsq(Ct,Ct_fit);

disp('done')
end

function Ct_model = modTofts_fun(b,inputs)

dt = diff([inputs(1,2),inputs(2,2)]);

% RTofts = Ktrans*exp(-Ktrans*t/ve);
% Ct_fit = vp*Cp + conv(Cp,RTofts);
%Ct_model = b(3)*Cp + conv(Cp,b(1)*exp(-b(1)*t/b(2)));

Ct_model_conv = conv(inputs(:,1),b(1)*exp(-b(1)*inputs(:,2)/b(2)))*dt;

Ct_model = b(3)*inputs(:,1) + Ct_model_conv(1:length(inputs(:,2)));

end

2CXM

function [vp,PS,ve,Fp,k01,k12,k21,rsq,Ct_fit] = fit_2CXM(Ct,Cp,t)

% R2cxm = A*exp(-a*t)+(1-A)*exp(-b*t);
% Ct_fit = conv(Fp*Cp,R2cxm);
% b(1) = A; b(2) = a; b(3) = b; b(4) = Fp

dt = diff([t(1),t(2)]);
```

```
inputs = [Cp(:),t(:)];

Ct_model = @TwoCXM_fun;

llim = [0;0;0;0];
ulim = [1;1;1;1];

beta0 = [0.5;0.5;0.5;0.5];
%figure;plot(t,Ct_model(beta0,t));
% beta = nlinfit(inputs,Ct,Ct_model,beta0);
[beta,resnorm] = lsqcurvefit(Ct_model,beta0,inputs,Ct,llim,ulim);

A = beta(1);
a = beta(2);
b = beta(3);
Fp = beta(4);

k01 = A*(a-b)+b; k12 = a*b/k01; k21 = a+b-k12-k01;
vp = Fp/k01; PS = k21*vp; ve = PS/k12;

% display fit

Ct_fit_conv = conv(Fp*inputs(:,1),A*exp(-a*inputs(:,2))+(1-A)*exp(-b*
    inputs(:,2)))*dt;
Ct_fit = Ct_fit_conv(1:length(inputs(:,2)));
%figure;plot(t,Ct, '.',t,Ct_fit(1:length(t)));title('2CXM Model');legend
    ('Ct data','Ct fit');xlabel('Time (s)');ylabel('Concentration');

%figure;plot(t,Ct, '.',t,TwoCXM_fun(beta,inputs));title('2CXM Model');
    legend('Ct data','Ct fit');xlabel('Time (s)');ylabel('Concentration')
    ;

disp(['resnorm = ',num2str(resnorm)]);

rsq = find_rsq(Ct,Ct_fit);

disp('done')
end

function Ct_model = TwoCXM_fun(b,inputs)

dt = diff([inputs(1,2),inputs(2,2)]);
```



```
% R2cxm = A*exp(-a*t)+(1-A)*exp(-b*t);
% Ct_fit = conv(Fp*Cp,R2cxm);
% b(1) = A; b(2) = a; b(3) = b; b(4) = Fp

% Ct_model = @(b,t) conv(Cp,Ktrans*exp(-Ktrans*t/ve));
% Ct_model = @(b,t) conv(Cp,b(1)*exp(-b(1)*t/b(2)))*dt;

Ct_model = conv(b(4)*inputs(:,1),b(1)*exp(-b(2)*inputs(:,2))+(1-b(1))*
    exp(-b(3)*inputs(:,2)))*dt;

Ct_model = Ct_model(1:length(inputs(:,2)));

end
```

Uptake Model

```
function [vp,PS,Fp,y,rsq,Ct_fit] = fit_uptake(Ct,Cp,t)

% Ruptake = (1-B)*exp(-y*t)+B;
% Ct_fit = conv(Fp*Cp,Ruptake);
% b(1) = B; b(2) = y; b(3) = Fp;

% R2cxm = A*exp(-a*t)+(1-A)*exp(-b*t);
% Ct_fit = conv(Fp*Cp,R2cxm);
% b(1) = A; b(2) = a; b(3) = b; b(4) = Fp

dt = diff([t(1),t(2)]);

inputs = [Cp(:),t(:)];

Ct_model = @uptake_fun;

l1im = [0;0;0];
ulim = [1;1;1];

beta0 = [0.5;0.5;0.5];
%figure;plot(t,Ct_model(beta0,t));
% beta = nlinfit(inputs,Ct,Ct_model,beta0);
[beta,resnorm] = lsqcurvefit(Ct_model,beta0,inputs,Ct,l1im,ulim);

B = beta(1);
```

```
y = beta(2);
Fp = beta(3);

% B=k21/(k01+k21); % ?
vp = Fp/(y*(1-B)); PS = B*Fp/(1-B);

% display fit

Ct_fit_conv = conv(Fp*inputs(:,1),(1-B)*exp(-y*inputs(:,2))+B)*dt;
Ct_fit = Ct_fit_conv(1:length(inputs(:,2)));
%figure;plot(t,Ct, '.',t,Ct_fit(1:length(t)));title('Uptake Model');
    legend('Ct data','Ct fit');xlabel('Time (s)');ylabel('Concentration')
    ;

%figure;plot(t,Ct, '.',t,uptake_fun(beta,inputs));title('Uptake Model');
    legend('Ct data','Ct fit');xlabel('Time (s)');ylabel('Concentration')
    ;

rsq = find_rsq(Ct,Ct_fit);
%disp(['rsq = ',num2str(rsq)]);

disp('done')
end

function Ct_model = uptake_fun(b,inputs)

dt = diff([inputs(1,2),inputs(2,2)]);

% Ruptake = (1-B)*exp(-y*t)+B;
% Ct_fit = conv(Fp*Cp,Ruptake);
% b(1) = B; b(2) = y; b(3) = Fp;

Ct_model = conv(b(3)*inputs(:,1),(1-b(1))*exp(-b(2)*inputs(:,2))+b(1))*
    dt;

Ct_model = Ct_model(1:length(inputs(:,2)));

end
```

A2.4 Processing Multiple Exams

BBB_2020_batch.m

Applies BBB_2020.m to all exams in folder BBB_exams

```
function BBB_2020_batch

% be in DATA folder

% experiment = dir('BBB_exams/exam_*');
experiment = dir('BBB_exams/exam_*');

for i = 1:length(experiment)

    close all
    exam = experiment(i).name;
    disp(exam);
    exam = num2str(exam(6:end));
    disp(exam);
    disp(' ');
    tic
    BBB_2020(exam);

    toc
end

disp(' ---- END ---- ')

end
```

A2.5 Consolidating Results

```
% processing those results
function processing_results()

root = [pwd filesep 'BBB_exams/'];
% pwd is DATA folder
% root = '/Users/ashleygilbank/Documents/DATA/BBB_exams/'; % since I
    should be there every time? will this work?

reg_reference = 1;
```

```
if reg_reference == 1
    direc = 'regMNI/';
else
    direc = 'regSELF/';
end

experiment = dir('BBB_exams/exam_*');

% saving_results('amygdala-L',experiment,root,direc)
% saving_results('amygdala-R',experiment,root,direc)
% saving_results('putamen-L',experiment,root,direc)
% saving_results('putamen-R',experiment,root,direc)
% saving_results('cerebellum',experiment,root,direc)
%
% saving_results('HofCN-L',experiment,root,direc)
% saving_results('HofCN-R',experiment,root,direc)
% saving_results('hippocampus-L',experiment,root,direc)
% saving_results('hippocampus-R',experiment,root,direc)
% saving_results('thalamus-L',experiment,root,direc)
% saving_results('thalamus-R',experiment,root,direc)
saving_results('post_pituitary',experiment,root,direc)
saving_results('pons',experiment,root,direc)

disp(' ---- END ---- ')

end

function saving_results(method,experiment,root,direc)

num_exams = length(experiment);

data = zeros(num_exams,20);

exams =
    [8173;8239;8242;8437;8126;8342;8264;8475;8405;8534;8569;8749;8461;8658;8685;8805;8
```

```
num_exams = length(exams);

for i = 1:num_exams

    %{
    exam = experiment(i).name;
    disp(exam);
    exam = num2str(exam(6:end));
    disp(exam);
    disp(' ');
    %}

    exam = num2str(exams(i)); % custom version
    disp(exam);
    disp(' ');

    exp = ['exam_' exam filesep];

    fpath = [root exp];
    folder1 = [fpath direc];

    cd(folder1)
    load([method '-results.mat'])
    cd('~\Documents\DATA')

    data(i,1) = rsq_Tofts;
    data(i,2) = rsq_modTofts;
    data(i,3) = rsq_2CXM;
    data(i,4) = rsq_uptake;
    data(i,5) = Ktrans_T;
    data(i,6) = Ktrans_mT;
    data(i,7) = PS_2;
    data(i,8) = PS_u;
    data(i,9) = ve_T;
    data(i,10) = ve_mT;
    data(i,11) = ve_2;
    data(i,12) = vp_mT;
    data(i,13) = vp_2;
    data(i,14) = vp_u;
    data(i,15) = Fp_2;
    data(i,16) = Fp_u;
    data(i,17) = k01_2;
    data(i,18) = k12_2;
    data(i,19) = k21_2;
```

```
data(i,20) = y_u;

end

X = [1 2 3 4];
X = repmat(X,[num_exams,1]);

figure;
for i=1:num_exams
    scatter(X(i,:),data(i,1:4));
    hold on;
%    exam = experiment(i).name;
%    disp(exam);
%    pause;
end
title(['R squared ( ' method ')']);ylabel('R squared');xlabel('Model (T,
mT,2,u)');ylim([0,1]);xlim([0,5])

writematrix(data,[method '.txt'])

disp(' ---- END ---- ')
end
```

Appendix B

Data

A1 Units and Exam Index

TABLE A2.1: Index for Parameter Units

Parameter	Description	Units
K^{trans}	Volume Transfer Rate	/s
PS	Permeability-Surface Area Product	mM/s
v_e	EES Volume Fraction	Unitless
v_p	Plasma Volume Fraction	Unitless
F_p	Plasma Perfusion	mM/s
z	Plasma Mean Transit Time	s

TABLE A2.2: Posterior Pituitary 1

Subject	First Scan	Second Scan
001	8173	N/A
002	8239	N/A
003	8242	8437
004	8126	8342
008	8264	8475
009	8405	8534
010	8569	8749
011	8461	8658

A2 Raw Data

TABLE A2.3: Posterior Pituitary 1

Exam	R^2_{Tofts}	R^2_{modTofts}	$R^2_{2\text{CXM}}$	R^2_{Uptake}	$K^{\text{trans}}_{\text{Tofts}}$	$K^{\text{trans}}_{\text{modTofts}}$	$\text{PS}_{2\text{CXM}}$	$\text{PS}_{\text{Uptake}}$
8173	0.975265267	0.975264847	0.975257645	0.975408624	0.006486279	0.006479231	3.83E-07	5.50E-06
8239	0.82506822	0.995079133	0.995078625	0.878953761	0.014928482	0.005068545	0.006643224	0.00031681
8242	0.694121858	0.694121907	0.694121577	0.746033296	0.002573809	0.002572337	3.06E-10	0.000122028
8437	0.766532326	0.805224929	0.86250272	0.847312276	0.017136019	0.007258742	0.001531664	0.000468642
8126	0.755052273	0.766822521	0.861330849	0.83237296	0.004354032	0.003695615	0.000849809	0.000166869
8342	0.879736279	0.952114976	0.959212734	0.927070596	0.013791622	0.00389954	0.001994567	0.00019196
8264	0.916095548	0.916095574	0.916080651	0.916095587	0.003641573	0.003642717	2.67E-09	1.47E-12
8475	0.937531079	0.93753108	0.937530781	0.93753108	0.004953818	0.004953754	2.40E-09	5.13E-13
8405	0.940620554	0.972850758	0.97331232	0.950277992	0.007365323	0.004651295	0.005037398	7.12E-05
8534	0.967929499	0.967929499	0.967929499	0.971728389	0.020684329	0.020684347	6.00E-12	5.24E-05
8569	0.901444426	0.984000395	0.986926959	0.945992041	0.015983821	0.005710463	0.004388205	0.000311126
8749	0.892239668	0.893901332	0.911186914	0.905811211	0.012362951	0.011380053	0.001374455	0.00016172
8461	0.887826627	0.915200879	0.986458913	0.981050568	0.007738614	0.005686155	0.000723442	0.000335469
8658	0.939109734	0.96184257	0.988376909	0.986276107	0.003980591	0.001168671	0.000110044	5.54E-05

TABLE A2.4: Posterior Pituitary 2

Exam	V_e, Tofts	$V_e, \text{modTofts}$	$V_e, 2\text{CXM}$	$V_p, \text{modTofts}$	$V_p, 2\text{CXM}$	V_p, Uptake	$F_p, 2\text{CXM}$	F_p, Uptake	Z_{Uptake}
8173	0.138607895	0.138549915	8.22E-06	0.000105832	0.138782755	0.137475226	0.006468343	0.006495674	0.047289758
8239	0.362049779	0.301128002	0.2892581	0.153190514	0.025454799	0.277669666	0.018655262	0.016913891	0.062054678
8242	0.172834959	0.172869197	2.06E-08	3.15E-08	0.172802433	0.144953338	0.002573307	0.002846781	0.020481138
8437	0.439130795	0.383510221	0.224220868	0.15152698	0.282352983	0.335953148	0.019302347	0.018761209	0.057239681
8126	0.322879841	0.312662881	0.149467056	0.018734931	0.19707862	0.25844347	0.00572188	0.00518273	0.020699301
8342	0.22721845	0.17656572	0.114424111	0.131500272	0.115560462	0.182793862	0.015164639	0.014515653	0.080460106
8264	0.118566182	0.118551739	8.78E-08	7.16E-09	0.118389742	0.118551528	0.003655542	0.003642735	0.03072702
8475	0.170933664	0.170934454	8.28E-08	2.20E-12	0.170970125	0.170934461	0.00495084	0.004953753	0.028980423
8405	0.186243793	0.167883269	0.107499823	0.040729927	0.073638202	0.170982698	0.008243595	0.007524859	0.044426024
8534	0.099418359	0.099418038	2.88E-11	8.76E-10	0.09941844	0.089303614	0.020684333	0.02042968	0.229352848
8569	0.331909229	0.277912334	0.200665959	0.143059126	0.128893004	0.260028331	0.018227363	0.017199629	0.06734172
8749	0.474795526	0.463375211	0.105306651	0.01952825	0.378653437	0.437508153	0.013457053	0.01286834	0.029782438
8461	0.350013454	0.33210744	0.177600146	0.041428687	0.250243615	0.274735235	0.008980873	0.00875235	0.033078463
8658	0.051521435	0.041195236	0.028530869	0.032820408	0.038650672	0.041497659	0.004009128	0.004007088	0.097896201

TABLE A2.5: Pons 1

Exam	R^2_{Tofts}	R^2_{modTofts}	$R^2_{2\text{CXM}}$	R^2_{Uptake}	$K^{\text{trans}}_{\text{Tofts}}$	$K^{\text{trans}}_{\text{modTofts}}$	$\text{PS}_{2\text{CXM}}$	$\text{PS}_{\text{Uptake}}$
8173	0.523432967	0.538933093	0.523446192	0.537901988	0.000626893	0.000325264	1.09E-08	4.70E-06
8239	0.841824907	0.962923695	0.841826398	0.946497621	0.001657055	7.53E-05	3.20E-19	2.51E-05
8242	0.354011341	0.700960063	0.789260138	0.760925781	0.000776908	0.000275261	0.000115957	5.24E-05
8437	0.350458021	0.785127686	0.786572181	0.693389136	0.001050221	0.000201837	0.000198533	5.26E-05
8126	0.86542287	0.86542287	0.865422291	0.866848684	0.000926003	0.000674248	0	1.06E-06
8342	0.243014785	0.275193219	0.277806365	0.25291363	0.000747708	0.000427426	0.000356255	7.59E-06
8264	0.289058369	0.33107049	0.289052893	0.316457752	0.000758785	0.000173181	8.63E-18	7.90E-06
8475	0.539420067	0.539420065	0.539416193	0.577403366	0.002092577	0.001527884	0	1.41E-05
8405	0.60976244	0.905118397	0.905117155	0.780610305	0.000466142	9.09E-05	0.000105875	1.49E-05
8534	0.812729927	0.812729927	0.812722322	0.818886262	0.001067739	0.000774017	0	3.40E-06
8569	0.587654643	0.700492452	0.587661487	0.692272981	0.001134599	0.000302932	7.06E-13	2.55E-05
8749	0.532506119	0.730119269	0.508339341	0.683411324	0.001847886	0.000134102	-3.64E-19	2.73E-05
8461	0.529178587	0.876955496	0.876957271	0.813930849	0.001335305	0.000211108	0.000235329	5.68E-05
8658	0.677988552	0.878082307	0.677993317	0.893197908	0.000538595	6.12E-05	3.33E-17	1.46E-05
8658	0.939109734	0.96184257	0.988376909	0.986276107	0.003980591	0.001168671	0.000110044	5.54E-05

TABLE A2.6: Pons 2

Exam	V_e, Tofts	$V_e, \text{modTofts}$	$V_e, \text{2CXM}$	$V_p, \text{modTofts}$	$V_p, \text{2CXM}$	V_p, Uptake	$F_p, \text{2CXM}$	F_p, Uptake	Z_{Uptake}
8173	0.009306348	0.007650689	4.88E-13	0.004605935	0.009285763	0.008366685	0.000807553	0.000807523	0.097055018
8239	0.014226426	0.014843801	6.75E-08	0.013136238	0.014045934	0.007121787	0.001317684	0.001347688	0.193570219
8242	0.022970052	0.022181103	8.01E-10	0.001503156	0.022888997	0.017854932	0.000413148	0.000474533	0.027783398
8437	0.016170945	0.013117133	0	0.008844704	0.002007927	0.010987786	0.001492467	0.000879899	0.082016475
8126	0.027049074	0.027045202	0.012993414	1.02E-07	0.018597575	0.021236386	0.000854815	0.000841082	0.040398514
8342	0.020357968	0.014750012	0.014084997	0.018815157	0.002333117	0.015461321	0.001976478	0.001973907	0.128995
8264	0.006939584	0.005495034	1.98E-09	0.004746053	0.006870621	0.005479788	0.0005178	0.000525259	0.097022311
8475	0.00318618	0.002614419	0	0.003228574	0.001158816	0.000796866	0.000868138	0.00079105	0.999993676
8405	0.00377465	0.003369513	9.41E-06	0.002654981	0.003439619	0.001858955	0.000276848	0.000294326	0.161803938
8534	0.000138921	9.06E-05	0	0.00202546	0.000644912	0.000644892	0.00064491	0.000644892	1
8569	0.010610324	0.008364622	9.58E-15	0.006666347	0.010534402	0.009258838	0.000840056	0.00084631	0.092091981
8749	0.015825992	0.014943828	2.67E-19	0.001700195	0.001793716	0.014073533	0.00133753	0.000560962	0.040384987
8461	0.024024965	0.021853319	2.32E-10	0.008393014	0.023891448	0.016968758	0.000859964	0.000956268	0.058286923
8658	0.003149797	0.006273363	-4.24E-19	0.006869979	0.003158568	0.001503936	0.00065276	0.000622085	0.418601716

TABLE A2.7: Cerebellum 1

Exam	R^2_{Tofts}	R^2_{modTofts}	R^2_{2CXM}	R^2_{Uptake}	$K^{\text{trans}}_{\text{Tofts}}$	$K^{\text{trans}}_{\text{modTofts}}$	PS_{2CXM}	PS_{Uptake}
8173	0.803026719	0.810028528	0.803028524	0.815699773	0.000805664	0.000403378	4.25E-14	4.51E-06
8239	0.670248987	0.949553872	0.670258384	0.882221934	0.001305461	0.000119499	6.37E-09	3.09E-05
8242	0.672199332	0.691851762	0.672262229	0.797814152	0.000408844	0.000346575	1.45E-11	2.15E-05
8437	0.66976969	0.79875788	0.197343328	0.799489893	0.000763414	0.000185131	0	2.13E-05
8126	0.536970181	0.536970955	0.620864052	0.608465751	0.000766416	0.000766696	5.21E-05	1.68E-05
8342	0.860018326	0.94025849	0.940258356	0.900418261	0.001912226	0.000307927	0.00034624	2.05E-05
8264	0.714692229	0.802188312	0.714696679	0.765841788	0.000511952	0.000115904	1.49E-10	6.40E-06
8475	0.804218125	0.80493084	0.803469316	0.853455365	0.000827853	0.00052989	0	5.81E-06
8405	0.247151771	0.460175836	0.246006202	0.352378043	0.000253137	4.04E-05	4.23E-06	6.46E-06
8534	0.828876858	0.828876859	0.828869064	0.828869058	0.000644911	0.00046526	0	2.61E-12
8569	0.892102191	0.931969302	0.892099415	0.90405769	0.000834084	0.000273868	7.64E-16	6.35E-06
8749	0.793681561	0.799224912	-0.517578096	0.817644775	0.00053252	0.000429677	1.99E-19	7.40E-06
8461	0.759199327	0.86120513	0.759198723	0.936810965	0.000850514	0.000308551	8.36E-12	3.28E-05
8658	0.911798178	0.973260962	0.911796626	0.972861861	0.00065305	9.90E-06	-8.77E-20	7.47E-06

TABLE A2.8: Cerebellum 2

Exam	V_e, Tofts	$V_e, \text{modTofts}$	$V_e, \text{2CXM}$	$V_p, \text{modTofts}$	$V_p, \text{2CXM}$	V_p, Uptake	$F_p, \text{2CXM}$	F_p, Uptake	Z_{Uptake}
8173	0.009306348	0.007650689	4.88E-13	0.004605935	0.009285763	0.008366685	0.000807553	0.000807523	0.097055018
8239	0.014226426	0.014843801	6.75E-08	0.013136238	0.014045934	0.007121787	0.001317684	0.001347688	0.193570219
8242	0.022970052	0.022181103	8.01E-10	0.001503156	0.022888997	0.017854932	0.000413148	0.000474533	0.027783398
8437	0.016170945	0.013117133	0	0.008844704	0.002007927	0.010987786	0.001492467	0.000879899	0.082016475
8126	0.027049074	0.027045202	0.012993414	1.02E-07	0.018597575	0.021236386	0.000854815	0.000841082	0.040398514
8342	0.020357968	0.014750012	0.014084997	0.018815157	0.002333117	0.015461321	0.001976478	0.001973907	0.128995
8264	0.006939584	0.005495034	1.98E-09	0.004746053	0.006870621	0.005479788	0.0005178	0.000525259	0.097022311
8475	0.00318618	0.002614419	0	0.003228574	0.001158816	0.000796866	0.000868138	0.00079105	0.999993676
8405	0.00377465	0.003369513	9.41E-06	0.002654981	0.003439619	0.001858955	0.000276848	0.000294326	0.161803938
8534	0.000138921	9.06E-05	0	0.00202546	0.000644912	0.000644892	0.00064491	0.000644892	1
8569	0.010610324	0.008364622	9.58E-15	0.006666347	0.010534402	0.009258838	0.000840056	0.00084631	0.092091981
8749	0.015825992	0.014943828	2.67E-19	0.001700195	0.001793716	0.014073533	0.00133753	0.000560962	0.040384987
8461	0.024024965	0.021853319	2.32E-10	0.008393014	0.023891448	0.016968758	0.000859964	0.000956268	0.058286923
8658	0.003149797	0.006273363	-4.24E-19	0.006869979	0.003158568	0.001503936	0.00065276	0.000622085	0.418601716

TABLE A2.9: Left Putamen 1

Exam	R^2_{Tofts}	R^2_{modTofts}	$R^2_{2\text{CXM}}$	R^2_{Uptake}	$K^{\text{trans}}_{\text{Tofts}}$	$K^{\text{trans}}_{\text{modTofts}}$	$\text{PS}_{2\text{CXM}}$	$\text{PS}_{\text{Uptake}}$
8173	0.208152016	0.29803146	0.208193315	0.293745803	0.000486037	0.000141328	4.18E-08	1.01E-05
8239	0.939358496	0.939358301	0.939358458	0.952542619	0.001408476	0.001408072	0	7.79E-06
8242	0.260372981	0.530663847	-1.6025432	0.314151036	0.000284247	0.000158587	-3.50E-19	3.22E-05
8437	0.051348641	0.587080954	0.587118596	0.48225043	0.00063968	0.000230581	0.000262899	7.03E-05
8126	0.08850689	0.381981513	0.384269228	0.351374016	0.000939093	8.28E-05	7.62E-05	2.88E-05
8342	0.163159685	0.188234298	0.203523703	0.186875524	0.000608362	0.000372044	0.000107468	1.03E-05
8264	0.081880997	0.125693688	0.081880742	0.110379214	0.000416119	0.000198445	9.17E-10	7.00E-06
8475	0.48257746	0.482577459	0.482572903	0.52839794	0.001071086	0.000781097	1.19E-19	8.58E-06
8405	0.220225036	0.502921081	0.572801331	0.521345771	0.000120931	4.36E-05	2.72E-05	1.02E-05
8534	0.775702352	0.775702352	0.775695952	0.787001507	0.00097843	0.000708649	0	4.26E-06
8569	0.626519157	0.63356334	0.626519073	0.632301436	0.000851251	0.000702669	0	8.26E-06
8749	0.136475789	0.529052774	0.529049824	0.459996274	0.00103237	0.000128089	0.000137376	4.79E-05
8461	0.903073217	0.903073221	0.90306911	0.903131598	0.001564967	0.001123291	0	8.35E-07
8658	0.365888363	0.60732194	0.721081447	0.712959777	0.000205539	6.74E-05	2.44E-05	1.52E-05

TABLE A2.10: Left Putamen 2

Exam	V_e, Tofts	$V_e, \text{modTofts}$	$V_e, 2\text{CXM}$	$V_p, \text{modTofts}$	$V_p, 2\text{CXM}$	V_p, Uptake	$F_p, 2\text{CXM}$	F_p, Uptake	Z_{Uptake}
8173	0.010734092	0.008719287	9.06E-07	0.005001618	0.010646056	0.008066356	0.000495033	0.000555374	0.070102306
8239	0.006262783	0.006263097	0	4.09E-06	0.006259415	0.005010263	0.0014087	0.001369312	0.274856971
8242	0.023616664	0.021069954	-4.69E-19	0.005139862	0.00157585	0.013526933	0.001176392	0.000461822	0.036521185
8437	0.041537184	0.037497958	0.03620691	0.013853868	0.004325482	0.019553551	0.001454079	0.001184636	0.064181669
8126	0.021681202	0.022522532	0.021869692	0.01354806	0.005768534	0.009287843	0.001252321	0.001259041	0.138655704
8342	0.017418747	0.015413518	0.00679784	0.003960121	0.010886107	0.015033434	0.000702175	0.000650425	0.043948342
8264	0.00994321	0.00860573	2.17E-08	0.00316861	0.009904578	0.008241175	0.000419444	0.000444166	0.054745479
8475	8.88E-05	0.00030086	1.19E-19	0.003269809	0.001071074	0.000966465	0.001071073	0.00095788	0.999999995
8405	0.00606179	0.00560144	0.0048381	0.001843546	0.002152818	0.002872037	0.000203059	0.00020368	0.074476202
8534	0.000379504	0.000106004	0	0.00304178	0.000978419	0.000927886	0.000978419	0.000923628	0.999999996
8569	0.026269517	0.024912653	0	0.002526065	0.026264138	0.024608951	0.000851677	0.000866128	0.035531181
8749	0.026493221	0.022212159	0.021933993	0.017048828	0.001778173	0.001895374	0.001639931	0.001847428	0.999992641
8461	2.63E-05	0.000131333	0	0.004979107	0.001564889	0.001558604	0.001564887	0.001557769	0.999999994
8658	0.00907567	0.008426655	0.009617408	0.003023674	0.004516289	0.0051037	0.000311025	0.000305457	0.062833013

TABLE A2.11: Right Putamen 1

Exam	R^2_{Tofts}	R^2_{modTofts}	$R^2_{2\text{CXM}}$	R^2_{Uptake}	$K^{\text{trans}}_{\text{Tofts}}$	$K^{\text{trans}}_{\text{modTofts}}$	$\text{PS}_{2\text{CXM}}$	$\text{PS}_{\text{Uptake}}$
8173	0.394839403	0.394839573	0.394839056	0.416794817	0.000612815	0.000613082	7.45E-10	4.90E-06
8239	0.916942917	0.94633406	0.915915195	0.942586482	0.001314849	2.29E-05	1.98E-19	9.11E-06
8242	0.609766627	0.691839421	0.609763092	0.677199253	0.000587391	0.000375506	8.41E-20	1.87E-05
8437	0.694060541	0.830752306	0.617611447	0.772467218	0.001032851	0.000107089	0	1.86E-05
8126	0.10432115	0.476673408	0.476669543	0.354460233	0.000671792	0.000120083	0.000130832	2.65E-05
8342	0.017738194	0.025281618	0.017792455	0.033054162	0.000463667	0.000287391	1.01E-06	6.35E-06
8264	0.18520305	0.200399137	0.185224983	0.233927153	0.0003453	9.12E-05	1.61E-10	5.06E-06
8475	0.551314368	0.551314368	0.551308843	0.552475117	0.000780888	0.000566783	8.67E-20	1.10E-06
8405	0.459401095	0.768101039	0.768100206	0.541684782	0.000192972	9.67E-05	0.000134509	9.61E-06
8534	0.834301797	0.834301799	0.834294077	0.834294073	0.000794659	0.000575341	-8.82E-20	1.48E-12
8569	0.756743959	0.822225536	0.756744162	0.767056771	0.000639157	0.000317673	7.57E-14	6.67E-06
8749	0.254939329	0.568690333	0.254891703	0.428720024	0.000973949	0.000176109	5.18E-12	3.74E-05
8461	0.725412601	0.89894425	0.898934783	0.875192059	0.001742675	9.66E-05	0.00010236	3.28E-05
8658	0.862093769	0.873997426	0.539643064	0.876993666	0.000219783	0.000118748	0	1.97E-06

*Master's of Applied Science– Ashley GILBANK; McMaster University– School of
Biomedical Engineering*

TABLE A2.12: Right Putamen 2

Exam	V_e , Tofts	V_e , modTofts	V_e , 2CXM	V_p , modTofts	V_p , 2CXM	V_p , Uptake	F_p , 2CXM	F_p , Uptake	$ZUptake$
8173	0.008507272	0.00850446	1.03E-08	4.39E-10	0.008509338	0.007608512	0.00061267	0.000606175	0.080315244
8239	0.004213708	0.004328901	2.65E-19	0.013624193	0.001787046	0.001264714	0.001336577	0.001255604	0.999999658
8242	0.024310031	0.021954514	3.44E-18	0.004447039	0.024231947	0.020150323	0.000592431	0.000637946	0.03258611
8437	0.01049359	0.008116263	0	0.011077417	0.001883011	0.001562995	0.001408944	0.001214197	0.788727102
8126	0.024672967	0.01851805	0.018255872	0.013447139	0.001444179	0.001560182	0.00131215	0.001533704	0.999999916
8342	0.009806823	0.008685337	1.80E-05	0.002483011	0.009722938	0.008379023	0.000472298	0.000485866	0.058743938
8264	0.004728983	0.003993808	2.19E-09	0.002871681	0.004701038	0.003716006	0.000347721	0.000344828	0.094157391
8475	8.57E-05	0.000163826	8.67E-20	0.002414071	0.000780882	0.000767366	0.00078088	0.000766266	0.999999861
8405	0.009934633	0.008658282	0.008423841	0.002498906	0.000457176	0.007269875	0.000318307	0.000244561	0.034961937
8534	0.000251769	7.34E-05	-8.82E-20	0.002472593	0.000794633	0.00079463	0.000794633	0.00079463	1
8569	0.015173567	0.012867058	1.78E-12	0.004909372	0.015131412	0.013652992	0.000642613	0.000665341	0.049220841
8749	0.023579086	0.017044578	1.17E-10	0.014514028	0.023116858	0.0031617	0.00101718	0.001744855	0.563710644
8461	0.012349342	0.014104415	0.013845796	0.017476862	0.00174895	0.001775857	0.001645828	0.00174308	0.99999962
8658	0.003278788	0.002817789	0	0.001227855	0.000451166	0.002899573	0.000338052	0.000223248	0.077672113

TABLE A2.13: Left Amygdala 1

Exam	R^2 _{Tofts}	R^2 _{modTofts}	R^2 _{2CXM}	R^2 _{Uptake}	K^{trans} _{Tofts}	K^{trans} _{modTofts}	PS _{2CXM}	PS _{Uptake}
8173	0.67257968	0.681313725	0.672580879	0.681678111	0.000883703	0.000454062	1.28E-08	4.21E-06
8239	0.835327251	0.960039897	0.835328423	0.955133331	0.001456751	5.51E-05	3.63E-17	2.34E-05
8242	0.249044847	0.485545999	-1.15392774	0.298689387	0.00018227	9.60E-05	-2.03E-19	1.32E-05
8437	-0.014680882	0.544284865	-0.196569369	0.308859156	0.000208541	8.19E-05	0	3.34E-05
8126	0.858776904	0.963495623	0.963495821	0.944389756	0.004563613	0.000218715	0.000226094	4.10E-05
8342	0.285372485	0.294837066	0.28541596	0.285373679	0.00133312	0.000662526	1.58E-06	1.01E-10
8264	-0.071931515	0.000342529	0.017543965	-0.010173006	0.000485084	0.000184465	8.05E-05	1.28E-05
8475	0.556479056	0.556479056	0.556474031	0.569869015	0.001467719	0.001066753	-1.63E-19	6.65E-06
8405	-0.091908845	0.170446259	0.21118376	0.117631184	5.43E-05	2.27E-05	1.69E-05	4.80E-06
8534	0.516864524	0.516864533	0.516861129	0.712436857	0.000376496	0.000276046	0	5.88E-06
8569	0.758107043	0.775506242	0.758100455	0.78286279	0.000557549	0.000379296	3.23E-10	8.51E-06
8749	0.665036694	0.665036694	0.665030548	0.713882238	0.002637656	0.001937846	2.93E-19	1.90E-05
8461	0.899148929	0.899148906	0.899146351	0.911556054	0.001388475	0.001008467	0	7.19E-06
8658	0.437058342	0.718496992	0.437493501	0.776087607	0.000122582	1.88E-05	7.23E-08	5.90E-06

TABLE A2.14: Left Amygdala 2

Exam	V_e , Tofts	V_e , modTofts	V_e , 2CXM	V_p , modTofts	V_p , 2CXM	V_p , Uptake	F_p , 2CXM	F_p , Uptake	$ZUptake$
8173	0.011199115	0.009390333	1.58E-07	0.004959952	0.011186898	0.010296168	0.00088485	0.000889262	0.086776869
8239	0.010494324	0.012655268	2.61E-16	0.014993191	0.010475572	0.006454146	0.001457757	0.001390946	0.219130688
8242	0.012928095	0.011272521	-2.72E-19	0.003111004	0.000915416	0.009515237	0.000684635	0.00022864	0.025418987
8437	0.016333345	0.01478341	0	0.005178052	0.013464812	0.001328478	0.000346678	0.00064496	0.510665043
8126	0.03460264	0.029633988	0.029193449	0.047472114	0.00465722	0.021892552	0.004429361	0.004516174	0.208161067
8342	0.019606629	0.016116945	2.44E-05	0.00850606	0.019550263	0.019575707	0.001342681	0.001335904	0.068242933
8264	0.012536992	0.010754233	0.0067935	0.004559237	0.00638671	0.009333954	0.000567741	0.000542405	0.059483209
8475	0.000377825	0.000286298	-1.63E-19	0.004520871	0.001467724	0.001386334	0.001467709	0.001379687	0.999999896
8405	0.003144374	0.002747992	0.002259456	0.00092592	0.000984851	0.001457763	0.000102711	0.00010425	0.074808107
8534	0.00018635	0.000110418	0	0.001132381	0.000376477	0.000307837	0.000376475	0.00030196	0.999999993
8569	0.013470125	0.012267474	7.70E-09	0.002604844	0.013403272	0.011695102	0.000563321	0.000577197	0.050081535
8749	0.000145353	0.000216271	2.93E-19	0.007890366	0.00263782	0.002399534	0.002637683	0.002380521	1
8461	0.000338128	0.000555641	0	0.00428631	0.0013885	0.001335083	0.00138848	0.00132789	0.999999992
8658	0.003049377	0.00311694	1.68E-06	0.001619853	0.002915272	0.001644589	0.000134622	0.000154809	0.097718573

TABLE A2.15: Right Amygdala 1

Exam	R^2_{Tofts}	R^2_{modTofts}	$R^2_{2\text{CXM}}$	R^2_{Uptake}	$K^{\text{trans}}_{\text{Tofts}}$	$K^{\text{trans}}_{\text{modTofts}}$	$\text{PS}_{2\text{CXM}}$	$\text{PS}_{\text{Uptake}}$
8173	0.674475379	0.674474063	0.674475548	0.674448256	0.000594254	0.00059461	4.27E-17	1.33E-08
8239	0.947540499	0.979806506	0.947540595	0.977971539	0.001223156	1.68E-05	-2.41E-19	9.28E-06
8242	0.366963222	0.761081639	-0.334703569	0.568008213	0.000239176	6.91E-05	0	1.85E-05
8437	0.60945475	0.718215332	0.466625496	0.643723802	0.000562757	0.000128125	0	8.38E-06
8126	0.820371189	0.939341888	0.820372167	0.909887273	0.002658126	9.14E-05	-3.02E-19	2.05E-05
8342	0.075957587	0.092865318	0.075961018	0.091971422	0.000669848	0.000189796	4.19E-10	7.39E-06
8264	0.004559105	0.026815856	0.033820576	0.013227351	0.000610659	0.000236296	0.000102157	5.69E-06
8475	0.514716035	0.514716034	0.514710367	0.514772109	0.001317186	0.000955592	1.46E-19	6.86E-07
8405	-0.027820556	0.149619226	0.150657238	0.02365539	0.000239483	0.000131231	0.000162188	1.16E-05
8534	0.879431085	0.879431085	0.879425938	0.879422173	0.000842811	0.000611089	9.36E-20	5.63E-09
8569	0.375135486	0.667754744	0.375063484	0.543310309	0.000289344	0.000113073	4.09E-08	1.58E-05
8749	0.122797323	0.593484913	-0.14869384	0.501076909	0.000607775	9.35E-05	2.46E-19	3.12E-05
8461	0.81365389	0.934989438	0.7991566	0.908748131	0.001383553	8.09E-05	0	2.01E-05
8658	0.909197113	0.942616839	0.617081109	0.955440895	0.000259766	7.13E-05	0	3.51E-06

TABLE A2.16: Right Amygdala 2

Exam	V_e, Tofts	$V_e, \text{modTofts}$	$V_e, 2\text{CXM}$	$V_p, \text{modTofts}$	$V_p, 2\text{CXM}$	V_p, Uptake	$F_p, 2\text{CXM}$	F_p, Uptake	Z_{Uptake}
8173	0.006766989	0.006762418	4.85E-16	4.43E-07	0.006761775	0.00676254	0.000594757	0.000594372	0.087893852
8239	0.004339051	0.005210991	-8.52E-19	0.012829692	0.00433296	0.001178834	0.001223294	0.001169556	0.999999202
8242	0.009343861	0.007777833	0	0.003861746	0.000841936	0.001281122	0.00063027	0.000475516	0.385617362
8437	0.008775364	0.00618069	0	0.006263509	0.001261367	0.006253614	0.000943628	0.000646429	0.104709508
8126	0.011003071	0.014194699	-1.24E-18	0.025061253	0.010896932	0.002497336	0.002662069	0.002476838	0.999999825
8342	0.008791012	0.006677871	5.41E-09	0.005877046	0.008722359	0.00717575	0.000676023	0.000686678	0.096723429
8264	0.01027954	0.008605249	0.004567738	0.004700415	0.005914043	0.008927449	0.000644432	0.000629785	0.071182369
8475	2.08E-06	1.76E-05	1.46E-19	0.004077368	0.001317213	0.00130867	0.001317198	0.001307984	0.999999991
8405	0.013006139	0.01152659	0.010143116	0.002870679	0.002277223	0.009945489	0.000383933	0.000290319	0.030361258
8534	5.68E-05	0.000200513	9.36E-20	0.002612749	0.000842804	0.000842729	0.000842803	0.000842723	1
8569	0.011593664	0.009830071	1.31E-06	0.003827783	0.01142287	0.007163229	0.000301453	0.000401035	0.058197474
8749	0.018581855	0.014083861	3.29E-19	0.011279289	0.00221877	0.001277203	0.001660291	0.001246051	1
8461	0.008041724	0.008505982	0	0.013475532	0.002038115	0.001376857	0.001524624	0.001356733	0.999999592
8658	0.00347078	0.002790485	0	0.002215596	0.000507774	0.002794211	0.000380427	0.000264833	0.0960359

TABLE A2.17: Left Thalamus 1

Exam	R^2_{Tofts}	R^2_{modTofts}	$R^2_{2\text{CXM}}$	R^2_{Uptake}	$K^{\text{trans}}_{\text{Tofts}}$	$K^{\text{trans}}_{\text{modTofts}}$	$\text{PS}_{2\text{CXM}}$	$\text{PS}_{\text{Uptake}}$
8173	0.44547691	0.52788969	0.44549676	0.530628094	0.000985936	0.000165037	1.31E-15	1.34E-05
8239	0.738205329	0.92775195	0.738205914	0.925558643	0.001707676	4.22E-05	5.71E-11	3.20E-05
8242	0.406774711	0.406834568	0.406835202	0.473779114	0.000468411	0.000471987	1.12E-08	2.66E-05
8437	0.304842105	0.650968385	0.6927376	0.656307317	0.000860798	0.000228664	0.00014505	6.07E-05
8126	0.737620447	0.745169397	0.737539459	0.764375507	0.000862874	0.000535599	9.90E-15	7.03E-06
8342	0.658577224	0.662463487	0.65857564	0.65901617	0.000806992	0.000572492	1.51E-12	1.59E-06
8264	0.719587341	0.757500031	0.719588199	0.740217985	0.000648637	0.000185514	2.26E-19	5.20E-06
8475	0.80334419	0.803344156	0.803342949	0.833118543	0.001216397	0.000887144	1.35E-19	6.79E-06
8405	0.532013038	0.741692538	0.743216312	0.673403688	0.000418971	7.61E-05	7.16E-05	1.28E-05
8534	0.735923814	0.735923824	0.735915889	0.735915829	0.0008027	0.000578975	0	9.81E-12
8569	0.439476372	0.486805943	0.439478307	0.44707608	0.001087914	0.000485911	7.32E-12	9.70E-06
8749	-0.05288707	0.129746617	0.204783089	0.204527346	0.000430539	0.000171633	7.56E-05	6.70E-05
8461	0.839907304	0.886646201	0.839916607	0.885536651	0.001400148	0.000396881	1.31E-08	2.00E-05
8658	0.658135403	0.809103083	0.835732834	0.829533772	0.000460529	5.71E-05	2.47E-05	1.28E-05

TABLE A2.18: Left Thalamus 2

Exam	$V_e, Tofts$	$V_e, modTofts$	$V_e, 2CXM$	$V_p, modTofts$	$V_p, 2CXM$	$V_p, Uptake$	$F_p, 2CXM$	$F_p, Uptake$	Z_{Uptake}
8173	0.013139868	0.010126001	1.73E-14	0.009778237	0.013061264	0.010065524	0.000993413	0.001017777	0.102450998
8239	0.010126447	0.028874076	3.38E-10	0.017153036	0.010115429	0.004112112	0.001708156	0.001578359	0.391617039
8242	0.029279365	0.029205854	6.86E-07	2.16E-07	0.029154056	0.022790769	0.000474482	0.00055199	0.025387909
8437	0.036141906	0.032675448	0.03011159	0.014748153	0.014127825	0.018885372	0.001372457	0.001315089	0.072847008
8126	0.015052056	0.0134244	1.69E-13	0.004185124	0.014919031	0.012999235	0.000873633	0.000870358	0.067495596
8342	0.013122311	0.01185344	2.44E-11	0.003001598	0.013103634	0.012784073	0.000808776	0.000810803	0.06354718
8264	0.008165852	0.006419351	2.82E-18	0.00542707	0.00813504	0.007065778	0.000651207	0.000652358	0.093062906
8475	0.00076909	0.000690371	1.35E-19	0.003712335	0.001216385	0.001133444	0.001216383	0.001126659	0.999999993
8405	0.007707601	0.007201611	0.006352587	0.004449795	0.002267967	0.004550297	0.000467189	0.000471856	0.106516044
8534	0.000502814	1.80E-05	0	0.002522464	0.000802689	0.000802683	0.000802689	0.000802683	0.999999999
8569	0.022238731	0.01853714	1.48E-10	0.008528861	0.022159763	0.020086931	0.00109446	0.001120182	0.056249799
8749	0.039088376	0.039175176	0.127066638	0.010880316	0.016457957	0.017084364	0.000916593	0.000910502	0.057213881
8461	0.01840607	0.014565308	1.70E-07	0.012292804	0.018317154	0.014645516	0.001406609	0.001428045	0.098869643
8658	0.007277352	0.00652185	0.006681384	0.00518641	0.003866328	0.004470929	0.000502178	0.000503994	0.115596833

TABLE A2.19: Right Thalamus 1

Exam	R^2_{Tofts}	$R^2_{modTofts}$	R^2_{2CXM}	R^2_{Uptake}	K^{trans}_{Tofts}	$K^{trans}_{modTofts}$	PS_{2CXM}	PS_{Uptake}
8173	0.512316851	0.512292388	0.512316662	0.524179569	0.000774294	0.000766369	0	4.63E-06
8239	0.847660866	0.913247499	0.845766651	0.908769842	0.001673351	3.42E-05	-2.54E-19	1.75E-05
8242	0.586977545	0.586977922	0.586969338	0.637740764	0.000687245	0.000687532	-1.22E-19	2.40E-05
8437	0.480754571	0.699763915	0.731668981	0.698808297	0.001039714	0.000209949	0.000117942	3.94E-05
8126	0.774253305	0.77768711	0.774278964	0.774241927	0.000661186	0.000325458	4.50E-07	1.45E-08
8342	0.499325769	0.555285562	0.499422651	0.542893768	0.000784075	0.00034366	3.41E-07	1.34E-05
8264	0.813849679	0.813848018	0.813849596	0.822483304	0.000650892	0.000650239	0	3.19E-06
8475	0.906897324	0.941294054	0.900170856	0.92449075	0.001670694	6.85E-05	0	8.67E-06
8405	0.536916374	0.806663667	0.80666225	0.647289493	0.000305532	8.49E-05	0.000103194	1.16E-05
8534	0.81755028	0.81755028	0.817542725	0.817542721	0.000917105	0.000664724	0	2.44E-12
8569	0.555118073	0.61762774	0.25747716	0.577814877	0.000869248	0.000285209	-2.03E-19	1.01E-05
8749	0.055932704	0.150578336	0.237283871	0.237348445	0.000531647	0.000277781	6.29E-05	4.61E-05
8461	0.667134633	0.830951383	0.667109385	0.807420332	0.001223274	0.000214595	0	3.38E-05
8658	0.773415136	0.82593402	0.773395258	0.823296731	0.000309254	7.35E-05	0	4.53E-06

TABLE A2.20: Right Thalamus 2

Exam	$V_e, Tofts$	$V_e, modTofts$	$V_e, 2CXM$	$V_p, modTofts$	$V_p, 2CXM$	$V_p, Uptake$	$F_p, 2CXM$	$F_p, Uptake$	Z_{Uptake}
8173	0.010974105	0.010968013	0	6.93E-05	0.010964801	0.010022056	0.000775221	0.000778054	0.078095731
8239	0.005851841	0.009163564	-3.39E-19	0.016806616	0.002286827	0.001573926	0.001710981	0.001556475	0.999999973
8242	0.035079329	0.03507418	-6.18E-18	4.96E-09	0.035036232	0.029866042	0.000689667	0.000738022	0.025513777
8437	0.025616907	0.021911349	0.018378601	0.013783572	0.011860322	0.015642903	0.001312494	0.001279459	0.084310378
8126	0.007496162	0.00621127	5.06E-06	0.0038799	0.007471579	0.007467392	0.000663169	0.000663024	0.08879117
8342	0.01711055	0.014036435	7.38E-06	0.006620643	0.016989597	0.01377717	0.000796056	0.000858895	0.063312922
8264	0.006851213	0.006859088	0	1.93E-07	0.006848675	0.006270705	0.000651115	0.00064487	0.103346521
8475	0.008171944	0.004586368	0	0.01729119	0.002461172	0.002276645	0.001830495	0.001715864	0.757488129
8405	0.008546112	0.007231808	0.007042801	0.003785214	0.000525395	0.004951112	0.000420627	0.000406876	0.084517417
8534	8.68E-05	4.11E-05	0	0.002845591	0.000917094	0.000917093	0.000917094	0.000917093	1
8569	0.013322855	0.010396075	-2.73E-19	0.00753502	0.001826778	0.011130967	0.0013579	0.000895586	0.081363758
8749	0.033367234	0.029911151	0.041442091	0.007510409	0.019096193	0.02050159	0.000799619	0.000779033	0.040246286
8461	0.021347538	0.018359833	0	0.013787434	0.021133573	0.013766186	0.001239272	0.00135721	0.101042773
8658	0.003867805	0.003033747	0	0.002772956	0.003823205	0.002927984	0.000312894	0.000319643	0.110714231

TABLE A2.21: Left Head of Caudate Nucleus 1

Exam	R^2_{Tofts}	R^2_{modTofts}	$R^2_{2\text{CXM}}$	R^2_{Uptake}	$K^{\text{trans}}_{\text{Tofts}}$	$K^{\text{trans}}_{\text{modTofts}}$	$\text{PS}_{2\text{CXM}}$	$\text{PS}_{\text{Uptake}}$
8173	0.445716308	0.496530938	0.445711369	0.515891008	0.00070965	0.000120178	4.38E-10	9.07E-06
8239	0.927510675	0.954308758	0.927511034	0.95635658	0.001254331	1.56E-05	-1.70E-19	1.00E-05
8242	0.402944526	0.534836792	0.402944464	0.41647822	0.000221109	0.000141446	9.59E-11	8.05E-06
8437	0.336602564	0.63595178	-0.238278444	0.570731465	0.000609165	0.000137382	0	3.04E-05
8126	0.256708664	0.256736571	0.256736566	0.257718256	0.000291093	0.000288327	4.40E-19	9.08E-07
8342	0.776817472	0.822101937	0.64443529	0.815782012	0.001031269	0.000162961	0	1.02E-05
8264	0.298240135	0.372449582	0.298277202	0.309473181	0.000310708	0.000143707	5.87E-08	3.35E-06
8475	0.59226651	0.59226651	0.592262433	0.59486069	0.000712843	0.00052021	0	1.40E-06
8405	0.157778168	0.465195046	0.503946883	0.464602332	7.44E-05	3.30E-05	2.54E-05	1.19E-05
8534	0.726198773	0.726198773	0.72619197	0.726189729	0.000610248	0.000440228	0	5.48E-10
8569	0.629751353	0.664914272	0.664913531	0.636849884	0.000714643	0.000456571	0.000875171	7.87E-06
8749	0.306704397	0.536111577	0.548732873	0.502675581	0.000724825	0.000178246	0.000127832	3.29E-05
8461	0.930258884	0.930258873	0.930255765	0.93025005	0.001247194	0.000900946	0	1.13E-08
8658	0.52486022	0.687749674	0.736011145	0.724871018	0.000149826	4.53E-05	1.86E-05	8.32E-06

TABLE A2.22: Left Head of Caudate Nucleus 2

Exam	V_e, Tofts	$V_e, \text{modTofts}$	$V_e, 2\text{CXM}$	$V_p, \text{modTofts}$	$V_p, 2\text{CXM}$	V_p, Uptake	$F_p, 2\text{CXM}$	F_p, Uptake	Z_{Uptake}
8173	0.009294898	0.00723169	5.68E-09	0.00689985	0.00924861	0.007336338	0.000714145	0.000721131	0.099531603
8239	0.006140776	0.008781519	-8.31E-19	0.013590649	0.006130199	0.004436548	0.001254644	0.00120923	0.274825764
8242	0.014723881	0.013134025	6.33E-09	0.002661368	0.014693489	0.012849531	0.000222509	0.000242097	0.019467705
8437	0.019110307	0.016045868	0	0.009462275	0.002068992	0.010164251	0.001542176	0.000881464	0.089708082
8126	0.005246973	0.005280788	8.05E-18	4.81E-11	0.005280892	0.005045314	0.000288319	0.000286965	0.05705745
8342	0.010412967	0.007120389	0	0.010206098	0.001872573	0.008227691	0.001400016	0.001041339	0.127806727
8264	0.007567647	0.006334558	1.37E-06	0.002602913	0.007531578	0.006698955	0.000313791	0.000329021	0.04961553
8475	0.000135786	6.05E-07	0	0.002171945	0.000712848	0.00069561	0.000712841	0.000694208	0.99999742
8405	0.006340482	0.006085343	0.005950258	0.001593668	0.001640866	0.002167727	0.000169429	0.000172304	0.084996096
8534	4.70E-05	0.000103923	0	0.001917021	0.000610273	0.000610213	0.000610271	0.000610212	0.999999996
8569	0.021256183	0.018753583	0.017374526	0.004557246	0.001782787	0.019609988	0.000860609	0.000733611	0.037811168
8749	0.024205759	0.019604015	0.016521115	0.011224923	0.008830692	0.01437961	0.001090095	0.001012895	0.072725699
8461	0.000259598	0.000317244	0	0.003905054	0.001247248	0.001247073	0.001247228	0.001247062	1
8658	0.005191184	0.004526153	0.004078381	0.002010431	0.002387259	0.002975392	0.000216262	0.00021133	0.073822513

TABLE A2.23: Right Head of Caudate Nucleus 1

Exam	R^2_{Tofts}	R^2_{modTofts}	$R^2_{2\text{CXM}}$	R^2_{Uptake}	$K^{\text{trans}}_{\text{Tofts}}$	$K^{\text{trans}}_{\text{modTofts}}$	$\text{PS}_{2\text{CXM}}$	$\text{PS}_{\text{Uptake}}$
8173	0.433420173	0.433420062	0.433416191	0.439198012	0.000461033	0.000461159	1.58E-14	2.25E-06
8239	0.882636049	0.941006368	0.88263711	0.938293585	0.001181733	2.11E-05	-2.47E-19	1.19E-05
8242	0.351245292	0.517403703	0.351232387	0.441341986	0.000442952	0.000274389	6.05E-10	2.24E-05
8437	0.767360795	0.873692574	0.692486302	0.816700187	0.000619979	7.52E-05	0	7.37E-06
8126	0.18188427	0.181912664	0.181909816	0.181913213	0.000101757	0.000100568	0	9.58E-11
8342	0.644002929	0.722674198	0.779518551	0.775944276	0.000728256	0.000109731	2.59E-05	1.45E-05
8264	0.565638948	0.631867277	0.565647067	0.606425024	0.000419373	0.000128507	1.22E-08	5.29E-06
8475	0.792801805	0.792985313	0.791224143	0.832136952	0.000592718	0.000368979	-6.87E-20	3.74E-06
8405	0.390794979	0.676251835	0.684902451	0.533036763	0.00012362	6.17E-05	6.11E-05	7.45E-06
8534	0.809811357	0.809811356	0.809804439	0.819629497	0.000729598	0.000528418	0	2.71E-06
8569	0.448574565	0.465274197	0.448584589	0.473417398	0.000400867	0.000305255	3.32E-14	7.84E-06
8749	0.153647633	0.382004384	-0.319019448	0.317029412	0.000627746	0.000141819	-2.58E-19	2.81E-05
8461	0.828156555	0.917009465	0.827019764	0.910304086	0.001492767	4.66E-05	-2.27E-19	1.82E-05
8658	0.77164055	0.830594632	0.771623856	0.836806693	0.000218565	7.50E-05	2.99E-20	4.68E-06

TABLE A2.24: Right Head of Caudate Nucleus 2

Exam	V _e , Tofts	V _e , modTofts	V _e , 2CXM	V _p , modTofts	V _p , 2CXM	V _p , Uptake	F _p , 2CXM	F _p , Uptake	ZUptake
8173	0.007590809	0.007589517	2.60E-13	1.45E-08	0.007579137	0.007159883	0.000462201	0.000460579	0.064642196
8239	0.00448897	0.006671002	-9.26E-19	0.012093552	0.004442661	0.0011233	0.001182986	0.001111439	0.999999992
8242	0.025527707	0.023044079	3.44E-08	0.004651209	0.025453626	0.020146297	0.000446729	0.000513076	0.026579821
8437	0.006279559	0.00455777	0	0.006570255	0.001127863	0.004324644	0.000844373	0.000662665	0.154935117
8126	0.001791188	0.001805894	0	6.01E-08	0.001817491	0.001808891	9.99E-05	0.000100302	0.055449267
8342	0.010454439	0.008307886	0.008128137	0.007738835	0.006820695	0.007387874	0.000751848	0.000752722	0.103848049
8264	0.006617829	0.0055333	1.91E-07	0.003526276	0.00658423	0.005386817	0.000422293	0.000434067	0.081562355
8475	0.002194054	0.001650822	-6.88E-20	0.00249644	0.000618794	0.00057249	0.000618339	0.000568749	0.99999646
8405	0.006420099	0.005716725	0.004730836	0.001543618	0.001637116	0.004298874	0.000195634	0.000167235	0.040635173
8534	0.000152845	0.000168348	0	0.002268421	0.000729597	0.000697366	0.000729595	0.000694652	0.999999889
8569	0.013367361	0.012437468	1.10E-12	0.00171483	0.013337852	0.011774285	0.000403308	0.000415957	0.035993247
8749	0.020051897	0.01540463	-3.45E-19	0.010200861	0.002319823	0.011197471	0.001733467	0.000911225	0.083891612
8461	0.005138775	0.007988283	-3.04E-19	0.014497073	0.00204453	0.001394338	0.001527888	0.001376182	0.999999874
8658	0.004352208	0.003637902	5.77E-19	0.001954711	0.00430448	0.003308804	0.000222697	0.00023911	0.073678735

TABLE A2.25: Left Hippocampus 1

Exam	R ² _{Tofts}	R ² _{modTofts}	R ² _{2CXM}	R ² _{Uptake}	K ^{trans} _{Tofts}	K ^{trans} _{modTofts}	PS _{2CXM}	PS _{Uptake}
8173	0.9269914	0.939661081	0.926991456	0.92778154	0.001806635	0.000396542	7.62E-10	2.19E-06
8239	0.775539668	0.962084149	0.775541484	0.946542654	0.001756191	7.49E-05	0	3.27E-05
8242	0.3884454	0.387780095	0.388367735	0.509981783	0.000276318	0.000274449	1.74E-13	1.46E-05
8437	0.231357703	0.430512635	-0.836395954	0.412767765	0.00051468	0.000187733	0	2.87E-05
8126	0.662289141	0.662289059	0.728226549	0.714550527	0.001153668	0.001153667	6.59E-05	1.92E-05
8342	0.782245899	0.831620172	0.837259275	0.806459604	0.001404641	0.000580072	0.000298335	1.55E-05
8264	0.650564125	0.715777166	0.650590587	0.692867765	0.000578382	0.000174012	3.19E-08	7.41E-06
8475	0.654723903	0.654718306	0.654722916	0.742702802	0.001119798	0.000820082	0	1.02E-05
8405	0.806249919	0.877647043	0.80625026	0.859792202	0.00051082	6.33E-05	0	7.01E-06
8534	0.857652467	0.857652467	0.857646951	0.85770344	0.001032766	0.00074851	0	3.79E-07
8569	0.634076534	0.718217126	0.634092735	0.658491808	0.001088467	0.000343032	3.84E-09	1.48E-05
8749	0.200103319	0.450888395	0.510834434	0.499149833	0.000888182	0.000156998	7.23E-05	4.07E-05
8461	0.799391292	0.867798684	0.799342991	0.857623703	0.001315543	0.00022435	0	2.05E-05
8658	0.70728761	0.8752291	0.707295873	0.893020362	0.000424937	4.49E-05	2.26E-08	1.13E-05

TABLE A2.26: Left Hippocampus 2

Exam	V _e , Tofts	V _e , modTofts	V _e , 2CXM	V _p , modTofts	V _p , 2CXM	V _p , Uptake	F _p , 2CXM	F _p , Uptake	ZUptake
8173	0.013608271	0.008745696	5.74E-09	0.015594531	0.013591813	0.013137144	0.001807963	0.001804504	0.137525899
8239	0.012630633	0.016953873	0	0.017526708	0.012608772	0.006803513	0.001757364	0.001663388	0.249295776
8242	0.013152234	0.013066092	7.75E-12	8.82E-05	0.012916057	0.009646101	0.000290563	0.000329041	0.035625339
8437	0.020901654	0.01776071	0	0.007417437	0.002038874	0.013228153	0.001510436	0.000692074	0.054486288
8126	0.038166555	0.03816646	0.015228194	4.24E-08	0.028328107	0.031900878	0.001231128	0.001212632	0.038614682
8342	0.026316199	0.021345081	0.012097417	0.011475277	0.013852758	0.022721999	0.001564095	0.001468142	0.065293615
8264	0.008737523	0.006957458	4.88E-07	0.00504375	0.008698841	0.007047883	0.000582007	0.000595568	0.085555146
8475	0.000207139	0.000488839	0	0.003393634	0.001119768	0.000995738	0.001119763	0.000985546	0.999999739
8405	0.005223256	0.004437485	0	0.00496406	0.005201944	0.003935661	0.000512223	0.000504872	0.130062547
8534	0.000125661	0.00010269	0	0.003204978	0.001032754	0.001028232	0.001032754	0.001027853	0.999999999
8569	0.019575026	0.01595574	6.74E-08	0.0099317	0.019421241	0.016053759	0.001101135	0.001153	0.072745076
8749	0.026532399	0.023785798	0.024729226	0.013432783	0.013729538	0.015777931	0.001147629	0.001126657	0.073988502
8461	0.015074438	0.011647149	0	0.013091811	0.014865883	0.01099018	0.001330247	0.00135166	0.12485224
8658	0.006134408	0.005758749	3.24E-07	0.004704675	0.006083678	0.003809409	0.000429307	0.000449771	0.121041954

TABLE A2.27: Right Hippocampus 1

Exam	R^2_{Tofts}	R^2_{modTofts}	$R^2_{2\text{CXM}}$	R^2_{Uptake}	$K^{\text{trans}}_{\text{Tofts}}$	$K^{\text{trans}}_{\text{modTofts}}$	$\text{PS}_{2\text{CXM}}$	$\text{PS}_{\text{Uptake}}$
8173	0.788617779	0.788502096	0.587872995	0.788618321	0.000487868	0.000484963	9.88E-20	9.98E-11
8239	0.918564331	0.972071937	0.918563843	0.959237607	0.001390713	4.36E-05	6.72E-15	1.30E-05
8242	0.706849759	0.730087273	0.706847462	0.744031949	0.000508553	0.000411191	8.87E-09	1.30E-05
8437	0.841050677	0.869161686	0.799061114	0.859359229	0.000959245	0.000116669	1.75E-19	6.55E-06
8126	0.802688447	0.802688237	0.802688737	0.80677	0.001068473	0.001068422	9.02E-09	4.80E-06
8342	0.794341436	0.846998971	0.794338836	0.804897144	0.001596222	0.00042288	4.46E-11	9.93E-06
8264	0.648268754	0.729043916	0.648278576	0.72660588	0.000471621	8.32E-05	6.72E-08	7.08E-06
8475	0.894811425	0.894984525	0.894437582	0.901074767	0.000949065	0.000610442	-1.45E-19	2.62E-06
8405	0.719819867	0.945060358	0.945058454	0.800540553	0.000456283	8.82E-05	0.000104103	1.02E-05
8534	0.884363202	0.884363202	0.884356723	0.884356611	0.001006925	0.000728897	0	2.59E-11
8569	0.813315731	0.87008696	0.810430874	0.842781664	0.000951877	0.00028591	1.29E-14	1.13E-05
8749	0.567607946	0.68139087	0.56690515	0.653386861	0.000981867	0.000400182	5.88E-09	2.17E-05
8461	0.573677973	0.86530769	0.338918191	0.829342965	0.000952581	9.79E-05	2.27E-19	3.28E-05
8658	0.919702336	0.919641867	0.919952409	0.924513272	0.000222272	0.000152627	3.11E-05	8.39E-07

TABLE A2.28: Right Hippocampus 2

Exam	V_e, Tofts	$V_e, \text{modTofts}$	$V_e, 2\text{CXM}$	$V_p, \text{modTofts}$	$V_p, 2\text{CXM}$	V_p, Uptake	$F_p, 2\text{CXM}$	F_p, Uptake	Z_{Uptake}
8173	0.005092159	0.005103333	1.32E-19	1.68E-05	0.000889796	0.005084713	0.000665122	0.000488504	0.096073173
8239	0.006395466	0.005971339	3.09E-14	0.014125566	0.006403145	0.002833812	0.00139053	0.001343088	0.478549116
8242	0.022892157	0.021732629	3.94E-07	0.002094455	0.022864567	0.020047038	0.000510265	0.00053977	0.027571692
8437	0.007314084	0.004431904	2.34E-19	0.009742259	0.001572283	0.006015206	0.001170579	0.000961092	0.160866728
8126	0.030458704	0.030459272	2.60E-07	4.76E-08	0.030454336	0.028964272	0.00106901	0.00107866	0.037406604
8342	0.019668632	0.014378052	5.36E-10	0.014429776	0.019561751	0.017243398	0.001605657	0.001639866	0.0956767
8264	0.006116579	0.004965202	4.86E-07	0.004529688	0.006086753	0.00461731	0.000474089	0.00047627	0.104681101
8475	0.00327456	0.002664111	-1.94E-19	0.003694754	0.001310108	0.000949179	0.000981237	0.000946562	0.999999699
8405	0.007445216	0.00635135	0.006150984	0.004783082	0.000618211	0.004435169	0.000512316	0.000528074	0.121366953
8534	8.08E-05	5.47E-05	0	0.003134763	0.001006913	0.001006907	0.001006913	0.001006907	0.999999999
8569	0.013998723	0.011473811	1.69E-13	0.008041817	0.013266243	0.011607968	0.001009141	0.000975701	0.085024978
8749	0.026063781	0.02062911	8.04E-09	0.010269282	0.025676573	0.020535306	0.001016853	0.001097227	0.054487519
8461	0.015269934	0.015452657	3.06E-19	0.011525541	0.002042929	0.006808268	0.001511932	0.001129511	0.170725279
8658	0.001524753	0.00129421	0.00020295	0.000777591	0.001272985	0.001393215	0.000221887	0.000219812	0.158375674

Bibliography

- Bazelaire, C. de, Siauve, N., Fournier, L., Frouin, F., Robert, P., Clement, O., Kerviler, E. de, and Cuenod, C. A. (2005). Comprehensive model for simultaneous MRI determination of perfusion and permeability using a blood-pool agent in rats rhabdomyosarcoma. *Eur Radiol* 15, 2497–2505.
- Brambilla, P., Glahn, D. C., Balestrieri, M., and Soares, J. C. (2005). Magnetic resonance findings in bipolar disorder. *Psychiatr Clin North Am.* 28(2), 443–67.
- Brix, G., Kiessling, F., Lucht, R., Darai, S., Wasser, K., Delorme, S., and Griebel, J. (2004). Microcirculation and microvasculature in breast tumors: pharmacokinetic analysis of dynamic MR image series. *Magn Reson Med* 52, 420–429.
- Chassidim, Y., Veksler, R., Lublinsky, S., Pell, G. S., Friedman, A., and Shelef, I. (2013). Quantitative imaging assessment of blood-brain barrier permeability in humans. *Fluids and barriers of the CNS* 10(1), 9.
- Daneman, R. and Prat, A. (2015). The blood-brain barrier. *Cold Spring Harbor perspectives in biology* 7(1).
- Dickie, B. R., Vandesquille, M., Ulloa, J., Boutin, H., Parkes, L. M., and M, P. G. J. (2019). Water-exchange MRI detects subtle blood-brain barrier breakdown in Alzheimer’s disease rats. *Neuroimage* 184, 349–358.
- Dieringer, M. A., Deimling, M., Santoro, D., Wuerfel, J., Madai, V. I., Sobesky, J., Knobelsdorff-Brenkenhoff, F. von, Schulz-Menger, J., and Niendorf, T. (2014). Rapid parametric mapping of the longitudinal relaxation time T1 using two-dimensional variable flip angle magnetic resonance imaging at 1.5 Tesla, 3 Tesla, and 7 Tesla. *PLoS One* 9(3).
- Donaldson, S. B., West, C. M., Davidson, S. E., Carrington, B. M., Hutchison, G., Jones, A. P., Sourbron, S. P., and Buckley, D. L. (2010). A comparison of tracer kinetic models for T1-weighted dynamic contrast-enhanced MRI: application in carcinoma of the cervix. *Magn Reson Med* 63(3), 691–700. Corrected in S. B. Donaldson, C. M. West, S. E. Davidson, B. M. Carrington, G. Hutchison, A. P. Jones, S. P. Sourbron, and D. L. Buckley. Erratum to a comparison of tracer kinetic models for T1-weighted dynamic contrast-enhanced MRI: Application in carcinoma of the cervix (*Magn Reson Med* 2010;63:691–700). *Magnetic Resonance in Medicine* 72 (3), 902–902.

Bibliography

- Elster, A. D. (2021). *Questions and Answers in MRI: MR Perfusion Overview*. URL: <http://mriquestions.com/dsc-v-dce-v-asl.html> (visited on 05/18/2021).
- Essig, M., Shiroishi, M. S., Nguyen, T. B., Saake, M., Provenzale, J. M., Enterline, D., Anzalone, N., Dörfler, A., Rovira, A., Wintermark, M., and Law, M. (2013). Perfusion MRI: the five most frequently asked technical questions. *Am J Roentgenol* 200(1), 24–34.
- Ferré, J. C., Bannier, E., Raoult, H., Mineur, G., Carsin-Nicol, B., and Gauvrit, J. Y. (2013). Arterial spin labeling (ASL) perfusion: techniques and clinical use. *Diagn Interv Imaging* 94(12), 1211–23.
- Frey, B., Noseworthy, M., Mishra, R., Kapczynski, F., and Minuzzi, L. (2017). A translational study of blood-brain barrier disruption in bipolar disorder: Implications for a new pathway for drug development. (*Physician Services Incorporated (PSI) Foundation*).
- Jahng, G. H., Li, K. L., Ostergaard, L., and Calamante, F. (2014). Perfusion magnetic resonance imaging: a comprehensive update on principles and techniques. *Korean J Radiol* 15(5), 554–77.
- Jenkinson, M. and Smith, S. (2001). A global optimisation method for robust affine registration of brain images. *Medical Image Analysis. Medical Image Analysis* 5(2), 143–156.
- Jenkinson M Bannister, P., Brady, J., and Smith, S. (2002). Improved optimisation for the robust and accurate linear registration and motion correction of brain images. *NeuroImage* 17(2), 825–841.
- Kamintsky, L., Cairns, K. A., Veksler, R., Bowen, C., Beyea, S. D., Friedman, A., and Calkin, C. (2020). Blood-brain barrier imaging as a potential biomarker for bipolar disorder progression. *NeuroImage: Clinical* 26, 102049. ISSN: 2213-1582.
- Lin, Z., Jiang, D., Liu, D., Li, Y., Uh, J., Hou, X., Pillai, J. J., Qin, Q., Ge, Y., and Lu, H. (2021). Noncontrast assessment of blood–brain barrier permeability to water: Shorter acquisition, test–retest reproducibility, and comparison with contrast-based method. *Mag Reson Med* 86(1), 143–156.
- McGehee, B. E., Pollock, J. M., and Maldjian, J. A. (2012). Brain perfusion imaging: How does it work and what should I use? *J Magn Reson Imaging* 36(6), 1257–72.
- Ohene, Y., Harrison, I. F., Evans, P. G., Thomas, D. L., Lythgoe, M. F., and Wells, J. A. (2021). Increased blood-brain barrier permeability to water in the aging brain detected using noninvasive multi-TE ASL MRI. *Magn Reson Med* (1), 326–333.
- Patel, J. P. and Frey, B. N. (2015). Disruption in the Blood-Brain Barrier: The Missing Link between Brain and Body Inflammation in Bipolar Disorder? *Neural Plasticity* 2015.

Bibliography

- Rohrer, M., Bauer, H., Mintonovitch, J., Requardt, M., and Weinmann, H. (2005). Comparison of magnetic properties of MRI contrast media solutions at different magnetic field strengths. *Invest Radiol* 40, 715–24.
- Smith, S. M., Jenkinson, M., Woolrich, M. W., Beckmann, C., Behrens, T. E. J., Johansen-Berg, H., Bannister, P., De Luca, M., Drobnjak, I., Flitney, D. E., Niazy, R., Saunders, J., Vickers, J., Zhang, Y., De Stefano, N., Brady, J. M., and Matthews, P. M. (2004). Advances in functional and structural MR image analysis and implementation as FSL. *NeuroImage* 23(S1), 208–19.
- Tofts, P. S. (1997). Modeling tracer kinetics in dynamic Gd-DTPA MR imaging. *J Magn Reson Imaging* 7, 91–101.
- Tofts, P. S., Berkowitz, B., and Schnall, M. D. (1995). Quantitative analysis of dynamic Gd-DTPA enhancement in breast tumors using a permeability model. *Magn Reson Med.* 33(4), 564–8.
- Tofts, P. S., Brix, G., Buckley, D. L., Evelhoch, J. L., Henderson, E., Knopp, M. V., Larsson, H. B., Lee, T., Mayr, N. A., Parker, G. J., Port, R. E., Taylor, J., and Weisskoff, R. M. (1999). Estimating kinetic parameters from dynamic contrast-enhanced T(1)-weighted MRI of a diffusible tracer: standardized quantities and symbols. *J Magn Reson Imaging* 10(3), 223–32.
- Tofts, P. S. and Kermode, A. G. (1991). Measurement of the blood-brain barrier permeability and leakage space using dynamic MR imaging. 1. Fundamental concepts. *Magn Reson Med.* 17(2), 357–67.
- Tofts, P. S., Shuter, B., and Pope, J. M. (1993). Ni-DTPA doped agarose gel-a phantom material for Gd-DTPA enhancement measurements. *Magn. Reson. Imaging* 11, 125–133.
- Wehrli, F. W., Duerk, J. L., and Hurst, G. C. (1990). Fast-scan magnetic resonance: principles and applications. *Magn Reson Q.* 6(3), 165–236.
- Weissberg, I., Veksler, R., Kamintsky, L., Saar-Ashkenazy, R., Milikovsky, D. Z., Shelef, I., and Friedman, A. (Nov. 2014). Imaging Blood-Brain Barrier Dysfunction in Football Players. *JAMA Neurology* 71(11), 1453–1455. ISSN: 2168-6149.
- Yuan, J., Chow, S. K. K., King, A. D., and Yeung, D. K. W. (2012). Heuristic linear mapping of physiological parameters in dynamic contrast-enhanced MRI without T1 measurement and contrast agent concentration. *J Magn Reson Imaging* 35(4), 916–925.